Comput. Methods Appl. Mech. Engrg. 417 (2023) 116411

Contents lists available at ScienceDirect

Comput. Methods Appl. Mech. Engrg.

journal homepage: www.elsevier.com/locate/cma

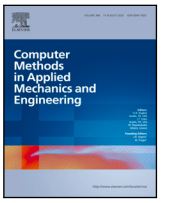

The entropy fix in augmented Riemann solvers in presence of source terms: Application to the Shallow Water Equations

Juan Mairal *, Javier Murillo, Pilar García-Navarro

I3A, Universidad de Zaragoza, C/Mariano Esquillor s/n, 50018, Zaragoza, Spain

ARTICLE INFO

Keywords:
Shallow Water Equations
Augmented Roe
HLLS
Source term
Entropy correction

ABSTRACT

Extensions to the Roe and HLL method have been previously formulated in order to solve the Shallow Water equations in the presence of source terms. These were named the Augmented Roe (ARoe) method and the HLLS method, respectively. This paper continues developing these formulations by examining how entropy corrections can be appropriately fitted in for the ARoe method and how the HLLS method can be formulated more generally. This is done in two ways. Firstly, this paper extends the reasoning of Harten and Hyman required by the ARoe method to include the source term contributions and thus arrives to a more complete formulation of the entropy fix, which will be compared with the approximation presented in previous works through numerical experiments. Secondly, it is shown how a relaxation of the criteria used when choosing waves in the HLLS method yields better solutions to problems where the HLLS would previously fail. In summary, this paper seeks to offer a comprehensible review of the ARoe and HLLS methods while improving its performance in cases with transcritical rarefactions for the inhomogeneous Shallow Water Equations in one dimension.

1. Introduction

The study of the dynamics of water with a free surface has direct applications to environmental research [1]. The behavior of water in rivers, basins, coasts and lakes is modeled in order to predict the evolution of floods, debris flows or tsunamis, which are some of the most destructive catastrophes [2] and are said to be now more frequent [3]. Additionally, open channel modeling is also a crucial step when designing hydraulic structures and operating them [4]. Therefore, scientists, public entities and companies are all invested in the development of the best predictive models for free surface flows. These models have often at their core the Shallow Water equations (SWE), which assume that flow acceleration is mostly confined to the directions parallel to the bed and the equations are vertically averaged. The SWE are a set of first order partial differential equations which, in general, are hyperbolic. It is common then to utilize conservative finite volume methods such as Godunov's scheme to solve these conservation laws.

In practical applications, source terms need to be taken into consideration. Whether by changes in the geometry or by the effect of friction, source terms are present in all SWE systems with any ambition to resemble a realistic case. The addition of sources causes the system of equations to lose its properties of strict hyperbolicity, and therefore the numerical methods used to solve them need to be more sophisticated. While it is true that sometimes a naive addition of the source term contribution to the scheme can yield good results, it might as well fail in some more complicated cases, inducing a degree of uncertainty. As a consequence, there is a great deal of research into theoretical test cases to ensure robustness and to appropriately introduce source terms [5]. In this regard, well-balanced upwind schemes [6–9] proved successful compared to point-centered schemes. These upwind schemes worked by reformulating the numerical flux to allow it to be balanced with the source term. In general, failure to converge to the physically

* Corresponding author.
E-mail address: mairalascaso@unizar.es (J. Mairal).

https://doi.org/10.1016/j.cma.2023.116411
Received 2 May 2023; Received in revised form 26 July 2023; Accepted 25 August 2023
Available online 15 September 2023

relevant solution has been the main problem when designing methods to solve conservation laws leading to the introduction of entropy corrections, of which the most well-known is the Harten–Hyman entropy fix [10], based on wave-splitting.

For the last two decades the consensus has been that well-balanced methods [11] work well to solve conservation laws with source terms. Indeed, the ability to preserve steady states even in the presence of geometrical discontinuities is the desired benchmark for these schemes [12–14]. Numerical schemes that exactly preserve the total head and the discharge in the simulation of smooth steady flows and that correctly dissipate mechanical energy in the presence of hydraulic jumps were presented for the first time in [15]. In [14], exactly energy balanced schemes were reviewed, and a comparison between a set of schemes from the literature was presented, including models that exactly preserve quiescent flows and models that exactly preserve moving-water steady flow, and among them, an energy balanced version of the augmented Roe (ARoe) solver presented in [16,17].

In the ARoe in [16] the source term was accounted for by increasing the number of elementary waves used to construct a Roe-type scheme, inspired by the ideas present in [18]. In the original formulation of the Roe Riemann solver [19], the approximate Riemann Problem (RP) is linearized leading to an approximate solution of the system with k equations, constituted by k waves that separate $k+1$ constant states, and the source term is discretized apart. In the ARoe solver [16], the source term is unified with the homogeneous part of the balance law and an approximated solution with one more wave of zero celerity and therefore one more inner constant state is achieved.

The strategies and results applied to the ARoe scheme can be also extended to construct energy balanced Harten–Lax–van Leer (HLL) [20] type methods. The HLL scheme computes directly an approximation to the inter-cell flux, only requiring estimates for the two largest signal speeds that bound the Riemann fan emerging from the initial discontinuity at the interface. Hence, HLL is a two-wave model approximate Riemann solver, only appropriate for hyperbolic systems with $k = 2$. If intermediate characteristic fields appear, such as contact surfaces in the case of jumps in concentrations or shear waves jumps in tangential velocity components, the more accurate HLLC method [21–24], a three-wave model where C stands for contact, is applicable. In [25] the number of waves in the well known HLL and HLLC solvers was extended to provide well-balanced versions called HLLS and HLLCS involving an stationary contact wave in the solution, that includes the presence of the source term. This new contact wave relates the approximate states at each side of the inter-cell wall through the contribution of the source term and requires choosing a local approximation of the determinant of the Jacobian. Typically [25], the ARoe eigenvalues are chosen since they can be computed easily but are also well known to perform badly in the presence of transcritical rarefactions.

This family of augmented solvers provide a description of the approximate solution of the Riemann problem and a straight forward evaluation of the inter-cell flux, and not only consider problems related with discontinuous bottom topography. The effect of numerical integration of the source term in the solution can be explored allowing to define appropriate properties representing the physical features associated with the problem. Augmented solvers such as ARoe and HLLS have been successfully developed during this last decade in the modeling of environmental problems in shallow flows including rainfall/runoff events [26], flood regulation [27], variable density [28] for erodible flows of one [29] or two layers, including loss of hyperbolicity [30], non-Newtonian rheologies [31] with accurate stop-and-go triggering mechanisms [32], dry granular free-surface transient flow [33], debris [34] and sediment transport in homogeneous [35] and heterogeneous [36] beds, thermally-driven and lava shallow flows [37], among others, and using first [38] or higher order of accuracy [39,40,31]. They also have been applied to the numerical simulation of blood flow in networks of arteries and veins [41–44].

However, the fact that the numerical flux is difficult to correct in order to single out the physical solutions is one of the main disadvantages of this philosophy [45], leading to undesirable consequences in presence of wet/dry fronts, as negative water depths. Some solutions to this issues where proposed, mainly reducing the time step to ensure convergence or the need to include tuning parameters. In all the previous applications of the ARoe and HLLS methods, the approximate Roe eigenvalues play an important role and may be observed when they do not represent correctly the features of the physical problem. The Roe method is only able to resolve discontinuous jumps, an therefore in transcritical rarefactions may fail, as the continuous fan of intermediate states is represented using a Roe eigenvalue with approximately zero velocity. This problem is revisited in presence of source terms under the perspective of the ARoe method. On the other hand, the HLLS is influenced not only by the selection of the wave speed estimates, but also by the evaluation of the determinant of the Jacobian. This paper is structured as follows. Section 2 presents the basic equations representing the physics of the model. Section 3 continues by introducing the numerical methods used to solve said equations, building the ARoe and HLLS methods from their basic principles. Then, Section 4 presents the corrections applied to the ARoe while Section 5 discusses the possible choices of wave speed estimates and linearized Jacobian for the HLLS solver. Finally, Section 6 contains numerical experiments involving challenging dynamical Riemann Problems extracted from [46] and steady-state cases of flow over a bump in order to test the effects of the discussed corrections over the augmented solvers. As pointed out in [14], the evaluation of the numerical models in the resonant regime is an important step when validating a numerical scheme. Section 7 presents the conclusions of this paper.

2. Mathematical model

2.1. 1D shallow water equations with source terms

In one dimension (1D) and assuming a frictionless channel of unit width, SWE are written as a conservation law as follows:

$$\frac{\partial \mathbf{U}}{\partial t} + \frac{\partial \mathbf{F}}{\partial x} = \mathbf{S}(\mathbf{U}), \tag{1}$$

where x is the coordinate along the channel, t is the time, $\mathbf{U}$ is the vector of conserved variables, $\mathbf{F}$ is the vector of fluxes, $\mathbf{S}$ is the source term, defined as:

$$\mathbf{U} = \begin{pmatrix} h \\ q \end{pmatrix}, \qquad \mathbf{F} = \begin{pmatrix} q \\ \frac{q^2}{h} + \frac{1}{2}gh^2 \end{pmatrix}, \qquad \mathbf{S} = \begin{pmatrix} 0 \\ \mathcal{T}(\mathbf{U}) \end{pmatrix} = \begin{pmatrix} 0 \\ -gh\frac{\partial z_b}{\partial x} \end{pmatrix}, \tag{2}$$

where h is the water depth, $q = hu$ is the unitary flow rate and u the cross sectional average velocity, g is the gravity acceleration and z_b is the bed level.

The source term $\mathbf{S}$ in this work focuses in the presence of discontinuous source terms, therefore, only changes in the bed level will be examined.

From the flux $\mathbf{F}$, the Jacobian matrix $\mathbf{J}$ of the equation can be found, with:

$$\mathbf{J} = \frac{\partial \mathbf{F}(\mathbf{U})}{\partial \mathbf{U}} = \begin{pmatrix} 0 & 1 \\ c^2 - u^2 & 2u \end{pmatrix}, \tag{3}$$

where $c = \sqrt{gh}$ is the speed of perturbations in the water. Then, the system can be rewritten as:

$$\frac{\partial \mathbf{U}}{\partial t} + \mathbf{J}\frac{\partial \mathbf{U}}{\partial x} = \mathbf{S}(\mathbf{U}). \tag{4}$$

If the homogeneous variant of the conservation law is strictly hyperbolic, then $\mathbf{J}$ has a distinct set of eigenvalues λ_k which in this case take the form:

$$\lambda_1 = u - c, \qquad \lambda_2 = u + c, \tag{5}$$

with eigenvectors $\mathbf{e}^k$:

$$\mathbf{e}^1 = \begin{pmatrix} 1 \\ \lambda_1 \end{pmatrix}, \qquad \mathbf{e}^2 = \begin{pmatrix} 1 \\ \lambda_2 \end{pmatrix}, \tag{6}$$

which can be organized into the matrix $\mathbf{P} = (\mathbf{e}^1, \mathbf{e}^2)$ so that the Jacobian can be diagonalized.

The relative sign of the eigenvalues determines the regime of the system, which can be subcritical if $\lambda_1\lambda_2 < 0$ or supercritical if $\lambda_1\lambda_2 > 0$. This is reflected into the Froude number, a dimensionless quantity which gives idea of the balance between inertial movement and gravity driven movement. It is defined as:

$$\mathrm{Fr} = \frac{u}{\sqrt{gh}} \tag{7}$$

The exact point (h, u) at which $\mathrm{Fr} = 1$ is the critical point, where the regime changes. In such circumstances, one of the eigenvalues becomes 0, which brings along some numerical problems, for which the entropy corrections are formulated. These kind of situations are the studied in this paper.

3. Numerical model

3.1. Homogeneous SWE

First, for the sake of completeness the system in (1) without source terms is considered:

$$\frac{\partial \mathbf{U}}{\partial t} + \mathbf{J}\frac{\partial \mathbf{U}}{\partial x} = 0. \tag{8}$$

To solve it, the domain is discretized so that between each two adjacent cells i and $i+1$ of constant length $\Delta x = x_{i+1} - x_i$ a local RP appears at each time step, defined as the following initial value problem (IVP):

$$\frac{\partial \mathbf{U}}{\partial t} + \mathbf{J}\frac{\partial \mathbf{U}}{\partial x'} = 0, \qquad \mathbf{U}(x', 0) = \begin{cases} \mathbf{U}_i & if \quad x' < 0 \\ \mathbf{U}_{i+1} & if \quad x' > 0 \end{cases} \tag{9}$$

where a new local coordinate $x' = x - x_{i+\frac{1}{2}}$ is defined for the ith local RP.

Constant vectors $\mathbf{U}_i = \mathbf{U}_i^n$ and $\mathbf{U}_{i+1} = \mathbf{U}_{i+1}^n$ are the initial conditions for the RP at time t^n at the left and right side of the discontinuity respectively, and are defined by averaging the solution in each cell:

$$\mathbf{U}_i^n = \frac{1}{\Delta x}\int_{x_{i-\frac{1}{2}}}^{x_{i+\frac{1}{2}}} \mathbf{U}(x, t = t^n)dx. \tag{10}$$

however, the RP will be solved using approximate linear solutions by means of Godunov's method, an explicit conservative method given by:

$$\mathbf{U}_i^{n+1} = \mathbf{U}_i^n - \frac{\Delta t}{\Delta x}\left[\mathbf{F}^-_{i+\frac{1}{2}} - \mathbf{F}^+_{i-\frac{1}{2}}\right]^n, \tag{11}$$

with $\mathbf{F}^{\pm}_{i\mp 1/2}$ the inter-cell numerical fluxes whose expression need to be found. The exact solution $\mathbf{U}(x, t)$ for this problem depends on the initial conditions and consists of a combination of possible wave patterns. In the subcritical case, they are (a) left rarefaction,

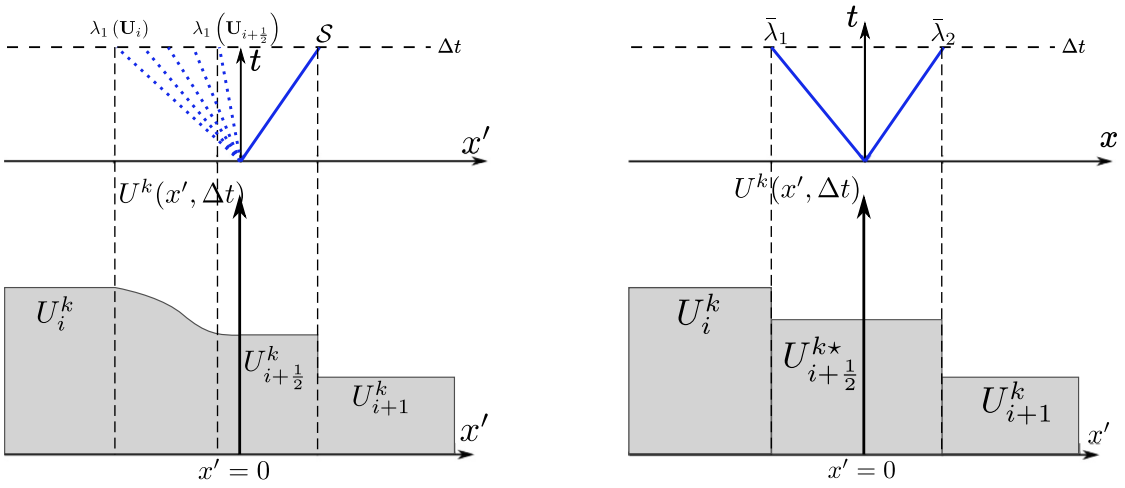

Fig. 1. Left: one of the possible solutions of the RP at time Δt. Right: approximation of left solution of the RP time Δt.

right shock (b) left shock, right rarefaction (c) left rarefaction, right rarefaction (d) left shock, right shock [47]. Fig. 1 pictures case (a) as an example. In the supercritical situations, waves travel in the same direction. Even when ignoring the exact solution $\mathbf{U}(x,t)$ of the RP, it is possible to estimate its variation around the inter-cell wall at a certain time step $\Delta t = t^{n+1} - t^n$ by integrating (9) over the control volume defined by $[-\frac{\Delta x}{2}, \frac{\Delta x}{2}] \times [t^n, t^n + \Delta t]$:

$$\int_{-\frac{\Delta x}{2}}^{\frac{\Delta x}{2}} \int_{t^n}^{t^{n+1}} \left(\frac{\partial \mathbf{U}}{\partial t} + \frac{\partial \mathbf{F}}{\partial x'} \right) dt dx' = 0. \tag{12}$$

Although the fluxes are not constant in time, it is assumed that they do not vary inside each time step Δt, leading to:

$$\int_{-\frac{\Delta x}{2}}^{\frac{\Delta x}{2}} \mathbf{U}(x',\Delta t) dx' = \frac{\Delta x}{2}\left(\mathbf{U}_{i+1} + \mathbf{U}_i\right) - \left(\mathbf{F}_{i+1} - \mathbf{F}_i\right)\Delta t, \tag{13}$$

where $\mathbf{F}_{i+1} = \mathbf{F}(\mathbf{U}_{i+1})$ and $\mathbf{F}_i = \mathbf{F}(\mathbf{U}_i)$. This assumption means that the accuracy order of the scheme must be one. All schemes used and mentioned in this work are first order.

The evolution of the RP is determined by the eigenvalues of the local Jacobian $\mathbf{J}_{i+\frac{1}{2}}$, where subscript $i+\frac{1}{2}$ implies that it depends on the values of $\mathbf{U}$ at each side of the inter-cell wall $x = x_{i+\frac{1}{2}}$, as pictured in Fig. 1. These eigenvalues $\left(\lambda_1, \lambda_2\right)_{i+\frac{1}{2}}$ are not determined since the conservative system is non-linear, and need to be approximated. A new linearized RP is introduced, where the local Jacobian has been linearized:

$$\frac{\partial \mathbf{U}}{\partial t} + \bar{\mathbf{J}}\left(\mathbf{U}_i, \mathbf{U}_{i+1}\right) \frac{\partial \mathbf{U}}{\partial x'} = 0, \qquad \mathbf{U}(x',0) = \begin{cases} \mathbf{U}_i & if \quad x' < 0 \\ \mathbf{U}_{i+1} & if \quad x' > 0 \end{cases}. \tag{14}$$

This yields a set of linear PDEs whose solution is known [16]. Information will travel in the (x,t) plane along lines of slope $x/t = \bar{\lambda}_k$ which will bound different constant states. Then, a weak solution is given by $\hat{\mathbf{U}}(x',\Delta t)$, a piecewise approximated solution at Δt constructed by different constant states separated by shock waves traveling with speed $\bar{\lambda}_k$ [11]. In the subcritical case, it can be written:

$$\hat{\mathbf{U}}(x',\Delta t) = \begin{cases} \mathbf{U}_i & if \quad x' < \bar{\lambda}_1 \Delta t \\ \mathbf{U}^\star_{i+\frac{1}{2}} & if \quad \bar{\lambda}_1 \Delta t < x' < \bar{\lambda}_2 \Delta t \\ \mathbf{U}_{i+1} & if \quad x' > \bar{\lambda}_2 \Delta t \end{cases} \tag{15}$$

The central approximate inter-cell state is obtained integrating (14) in a volume defined by the eigenvalues of the linearized Jacobian $\bar{\mathbf{J}}$, namely $[\bar{\lambda}_1 \Delta t, \bar{\lambda}_2 \Delta t]$ domain:

$$\mathbf{U}^\star_{i+\frac{1}{2}}(\bar{\lambda}_1, \bar{\lambda}_2, \Delta t) = \frac{1}{(\bar{\lambda}_2 - \bar{\lambda}_1)\Delta t} \int_{\bar{\lambda}_1 \Delta t}^{\bar{\lambda}_2 \Delta t} \mathbf{U}(x',\Delta t) dx' = \frac{\left(\bar{\lambda}_2 \mathbf{U}_{i+1} + \bar{\lambda}_1 \mathbf{U}_i\right) - \left(\mathbf{F}_{i+1} - \mathbf{F}_i\right)}{\bar{\lambda}_2 - \bar{\lambda}_1}, \tag{16}$$

This solution can be integrated in the $\left[-\frac{\Delta x}{2}, \frac{\Delta x}{2}\right]$:

$$\int_{-\frac{\Delta x}{2}}^{\frac{\Delta x}{2}} \hat{\mathbf{U}}(x',\Delta t) dx' = \left(\bar{\lambda}_1 \Delta t + \frac{\Delta x}{2}\right) \mathbf{U}_i + \Delta t \left(\bar{\lambda}_2 - \bar{\lambda}_1\right) \mathbf{U}^\star_{i+\frac{1}{2}} + \left(\frac{\Delta x}{2} - \bar{\lambda}_2 \Delta t\right) \mathbf{U}_{i+1}, \tag{17}$$

and then, since $\hat{\mathbf{U}}$ is a weak solution of the RP, then it must satisfy integral Eq. (13), leading to:

$$\mathbf{F}_{i+1} - \mathbf{F}_i = \bar{\lambda}_2 \left(\mathbf{U}_{i+1} - \mathbf{U}^{\star}_{i+\frac{1}{2}} \right) + \bar{\lambda}_1 \left(\mathbf{U}^{\star}_{i+\frac{1}{2}} - \mathbf{U}_i \right). \tag{18}$$

Then, the inter-cell flux can be computed from the contributions of each of the waves:

$$\mathbf{F}^{\star}_{i+\frac{1}{2}} = \mathbf{F}_i + \bar{\lambda}_1 \left(\mathbf{U}^{\star}_{i+\frac{1}{2}} - \mathbf{U}_i \right) = \mathbf{F}_{i+1} - \bar{\lambda}_2 \left(\mathbf{U}_{i+1} - \mathbf{U}^{\star}_{i+\frac{1}{2}} \right). \tag{19}$$

The question of linearizing the Jacobian remains open, as the weak solution in (15) has been achieved assuming that $\bar{\lambda}_k$ are known. This paper looks at the ARoe and HLLS methods to find suitable $\bar{\lambda}_k$.

3.2. Inhomogenous SWE

The source term is added to the right hand side of the conservation law in the Riemann problem:

$$\frac{\partial \mathbf{U}}{\partial t} + \mathbf{J} \frac{\partial \mathbf{U}}{\partial x'} = \mathbf{S}, \qquad \mathbf{U}(x', 0) = \begin{cases} \mathbf{U}_i & if \quad x' < 0 \\ \mathbf{U}_{i+1} & if \quad x' > 0 \end{cases}. \tag{20}$$

The solution of this problem will satisfy integral equation:

$$\int_{-\frac{\Delta x}{2}}^{\frac{\Delta x}{2}} \int_{t^n}^{t^{n+1}} \left(\frac{\partial \mathbf{U}}{\partial t} + \frac{\partial \mathbf{F}}{\partial x'} - \mathbf{S} \right) dt dx' = 0. \tag{21}$$

By again assuming the fluxes are constant in the time-step Δt:

$$\int_{-\frac{\Delta x}{2}}^{\frac{\Delta x}{2}} \mathbf{U}(x', \Delta t) dx = \frac{\Delta x}{2} \left(\mathbf{U}_{i+1} + \mathbf{U}_i \right) - \left(\mathbf{F}_{i+1} - \mathbf{F}_i \right) \Delta t + \int_{-\frac{\Delta x}{2}}^{\frac{\Delta x}{2}} \int_{t^n}^{t^{n+1}} \mathbf{S} dt dx', \tag{22}$$

where the change in time of the source term vector $\mathbf{S}$ is unknown. Therefore, a suitable time linearization is required:

$$\int_{-\frac{\Delta x}{2}}^{\frac{\Delta x}{2}} \int_{t^n}^{t^{n+1}} \mathbf{S} dt dx \approx \Delta t \bar{\mathbf{S}}_{i+\frac{1}{2}}, \tag{23}$$

with $\bar{\mathbf{S}}_{i+\frac{1}{2}} = [0, \bar{S}_{i+\frac{1}{2}}]^T$. The details of this linearization are discussed in Appendix A.

It is assumed that the action of the source term occurs only at the inter-cell wall [16], as a steady contact wave at $x' = 0$. By again introducing a linearized Jacobian natrux $\bar{\mathbf{J}}_{i+\frac{1}{2}} = \mathbf{J}\left(\mathbf{U}_{i+1}, \mathbf{U}_i \right)$, whose eigenvalues are $\bar{\lambda}_1$, $\bar{\lambda}_2$, locally defined at the $x' = 0$ wall, then the integral equation can be written:

$$\frac{\partial \mathbf{U}}{\partial t} + \bar{\mathbf{J}}\left(\mathbf{U}_i, \mathbf{U}_{i+1} \right) \frac{\partial \mathbf{U}}{\partial x'} = \bar{\mathbf{S}}_{i+\frac{1}{2}}, \qquad \mathbf{U}(x', 0) = \begin{cases} \mathbf{U}_i & if \quad x' < 0 \\ \mathbf{U}_{i+1} & if \quad x' > 0 \end{cases}. \tag{24}$$

This linearized RP is solved by constructing a weak solution in four parts, which in the subcritical regime is

$$\hat{\mathbf{U}}(x, \Delta t) = \begin{cases} \mathbf{U}_i & if \quad x' < \bar{\lambda}_1 \Delta t \\ \mathbf{U}^-_i & if \quad \bar{\lambda}_1 \Delta t < x' < 0 \\ \mathbf{U}^+_{i+1} & if \quad 0 < x' < \bar{\lambda}_2 \Delta t \\ \mathbf{U}_{i+1} & if \quad x' > \bar{\lambda}_2 \Delta t \end{cases}, \tag{25}$$

which needs to satisfy (22), leading to the condition:

$$\mathbf{F}_{i+1} - \mathbf{F}_i - \bar{\mathbf{S}}_{i+\frac{1}{2}} = \bar{\lambda}_2 \left(\mathbf{U}_{i+1} - \mathbf{U}^+_{i+1} \right) + \bar{\lambda}_1 \left(\mathbf{U}^-_i - \mathbf{U}_i \right). \tag{26}$$

This means that the change in homogeneous fluxes from one cell to the next is given by the waves as in (18). In constructing a piecewise approximate solution, the inter-cell state $\mathbf{U}^{\star}$ from the homogeneous case has been split in two approximate states $\mathbf{U}^-_i$ and $\mathbf{U}^+_{i+1}$. Reformulating the integral Eq. (22) between $[\bar{\lambda}_1 \Delta t, \bar{\lambda}_2 \Delta t]$ in order to solve for the two central states only leads to:

$$\int_{\bar{\lambda}_1 \Delta t}^{\bar{\lambda}_2 \Delta t} \mathbf{U}(x', \Delta t) dx' = \left(\bar{\lambda}_2 - \bar{\lambda}_1 \right) \left(\mathbf{U}^+_{i+1} - \mathbf{U}^-_i \right) \Delta t - \left(\mathbf{F}^+_{i+1} - \mathbf{F}^-_i - \bar{\mathbf{S}}_{i+\frac{1}{2}} \right) \Delta t. \tag{27}$$

While the same integration performed on the linearized system (24) allows to write:

$$\int_{\bar{\lambda}_1 \Delta t}^{\bar{\lambda}_2 \Delta t} \mathbf{U}(x', \Delta t) dx' = \left(\bar{\lambda}_2 - \bar{\lambda}_1 \right) \left(\mathbf{U}^+_{i+1} + \mathbf{U}^-_i \right) \Delta t - \bar{\mathbf{J}}_{i+\frac{1}{2}} \left(\mathbf{U}^+_{i+1} + \mathbf{U}^-_i \right) \Delta t - \bar{\mathbf{S}}_{i+\frac{1}{2}} \Delta t. \tag{28}$$

Subtracting equations Eqs. (27) and (28) leads to:

$$\mathbf{F}^+_{i+1} - \mathbf{F}^-_i = \bar{\mathbf{J}}_{i+\frac{1}{2}} \left(\mathbf{U}^+_{i+1} - \mathbf{U}^-_i \right). \tag{29}$$

Now, since a static shock wave is assumed between states $\mathbf{U}^+_{i+1}$ and $\mathbf{U}^-_i$, the Rankine–Hugoniot condition can be imposed with a wave speed $\sigma = 0$:

$$\mathbf{F}^+_{i+1} - \mathbf{F}^-_i - \bar{\mathbf{S}}_{i+\frac{1}{2}} = \sigma\left(\mathbf{U}^+_{i+1} - \mathbf{U}^-_i\right) = 0. \tag{30}$$

which, if substituted into (30), leads to the following result regarding the relationship between the source term and the approximate states at each side of the inter-cell wall:

$$\bar{\mathbf{J}}_{i+\frac{1}{2}}(\mathbf{U}^+_{i+1} - \mathbf{U}^-_i) = \bar{\mathbf{S}}_{i+\frac{1}{2}}. \tag{31}$$

Then, the inverse of the approximate Jacobian matrix:

$$\bar{\mathbf{J}}^{-1}_{i+\frac{1}{2}} = \frac{1}{\det \bar{\mathbf{J}}_{i+\frac{1}{2}}} \begin{pmatrix} 2\bar{u} & -1 \\ \bar{u}^2 - \bar{c}^2 & 0 \end{pmatrix} = \frac{1}{\bar{\lambda}_1\bar{\lambda}_2} \begin{pmatrix} 2\bar{u} & -1 \\ \bar{u}^2 - \bar{c}^2 & 0 \end{pmatrix}, \tag{32}$$

can be used on both sides of (31) to define the new vector $\bar{\mathbf{H}}$:

$$\mathbf{U}^+_{i+1} - \mathbf{U}^-_i = \bar{\mathbf{J}}^{-1}_{i+\frac{1}{2}} \begin{pmatrix} 0 \\ S_{i+\frac{1}{2}} \end{pmatrix} = -\frac{1}{\bar{\lambda}_1\bar{\lambda}_2} \begin{pmatrix} S_{i+\frac{1}{2}} \\ 0 \end{pmatrix} = \bar{\mathbf{H}}_{i+\frac{1}{2}}. \tag{33}$$

where it is important to remember that $\bar{\mathbf{J}}_{i+\frac{1}{2}}$ is a linearized Jacobian dependent on the initial values of the RP. The existence of $\bar{\mathbf{H}}_{i+\frac{1}{2}}$ requires the Jacobian to be invertible and $\bar{\mathbf{H}}_{i+\frac{1}{2}}$ provides a direct relationship between the two approximate inner states of the weak solution across the inter-cell wall.

Regardless, the inter-cell flux in the subcritical case can be computed from the contributions of each of the waves:

$$\mathbf{F}^-_{i+\frac{1}{2}} = \mathbf{F}_i + \bar{\lambda}_1\left(\mathbf{U}^-_{i+\frac{1}{2}} - \mathbf{U}_i\right) \neq \mathbf{F}^+_{i+\frac{1}{2}} = \mathbf{F}_{i+1} - \bar{\lambda}_2\left(\mathbf{U}_{i+1} - \mathbf{U}^+_{i+\frac{1}{2}}\right). \tag{34}$$

The supercritical case is included in Appendix B.

3.3. The augmented Roe solver

Now the choice of approximate Jacobian $\bar{\mathbf{J}}_{i+\frac{1}{2}}$ is discussed. It can be based on the so-called Roe averaged values between cells:

$$\tilde{\mathbf{J}} = \begin{pmatrix} 0 & 1 \\ \tilde{c}^2 - \tilde{u}^2 & 2\tilde{u} \end{pmatrix}, \qquad \tilde{h} = \frac{h_i + h_{i+1}}{2}, \qquad \tilde{u} = \frac{u_i\sqrt{h_i} + u_{i+1}\sqrt{h_{i+1}}}{\sqrt{h_i} + \sqrt{h_{i+1}}}, \tag{35}$$

where the tilde shall indicate that a certain variable is based on the Roe averaged values and thus always associated with an inter-cell wall. For the sake of clarity the $i + \frac{1}{2}$ subscript is implied but omitted. Additionally, the celerity is defined $\tilde{c} = \sqrt{g\tilde{h}}$. This constant matrix is diagonalizable with eigenvalues:

$$\tilde{\lambda}_1 = \tilde{u} - \tilde{c}, \quad \tilde{\lambda}_2 = \tilde{u} + \tilde{c}. \tag{36}$$

Their corresponding eigenvectors are:

$$\tilde{\mathbf{e}}^1 = \begin{pmatrix} 1 \\ \tilde{\lambda}_1 \end{pmatrix} \qquad \tilde{\mathbf{e}}^2 = \begin{pmatrix} 1 \\ \tilde{\lambda}_2 \end{pmatrix}, \tag{37}$$

which can be arranged into matrices $\tilde{\mathbf{P}} = (\tilde{\mathbf{e}}^1, \tilde{\mathbf{e}}^2)$ and $\tilde{\mathbf{P}}^{-1}$ with the following property:

$$\tilde{\mathbf{J}} = (\tilde{\mathbf{P}}\tilde{\mathbf{\Lambda}}\tilde{\mathbf{P}}^{-1}), \qquad \tilde{\mathbf{\Lambda}} = \begin{pmatrix} \tilde{\lambda}_1 & 0 \\ 0 & \tilde{\lambda}_2 \end{pmatrix}, \tag{38}$$

and system in (20) is transformed using $\tilde{\mathbf{P}}^{-1}$ matrix as into a decoupled system expressed in terms of the characteristic variables $\mathbf{V} = \tilde{\mathbf{P}}^{-1}\mathbf{U}$ the IVP is transformed in a set of two decoupled linear IVP's, with the following form:

$$\frac{\partial \mathbf{V}}{\partial t} + \tilde{\mathbf{\Lambda}}\frac{\partial \mathbf{V}}{\partial x} = \bar{\mathbf{B}}_{i+\frac{1}{2}}, \qquad \mathbf{V}(x', 0) = \begin{cases} \mathbf{V}_i = \tilde{\mathbf{P}}^{-1}\mathbf{U}_i & if \quad x' < 0 \\ \mathbf{V}_{i+1} = \tilde{\mathbf{P}}^{-1}\mathbf{U}_{i+1} & if \quad x' > 0 \end{cases}, \tag{39}$$

where $\bar{\mathbf{B}}_{i+\frac{1}{2}} = \tilde{\mathbf{P}}^{-1}_{i+\frac{1}{2}}\bar{\mathbf{S}} = [\bar{\beta}_1, \bar{\beta}_2]^T_{i+\frac{1}{2}}$ is the new transformed vector of source terms. Integration of (39) over control volume $[-\frac{\Delta x}{2}, \frac{\Delta x}{2}] \times [t^n, t^n + \Delta t]$ yields one equation for each component:

$$\int_{-\frac{\Delta x}{2}}^{\frac{\Delta x}{2}} V^k(x', \Delta t)dx = \frac{\Delta x}{2}\left(V^k_{i+1} + V^k_i\right) - \Delta t\tilde{\lambda}_k\left(V^k_{i+1} - V^k_i\right) + \Delta t\bar{\beta}_k. \tag{40}$$

where in this case $k = 1, 2$. A weak solution $\hat{V}^k$ is proposed for each characteristic variable following the reasoning in Section 3.2. Two cases are possible as $\tilde{\lambda}_k$ can be either negative or positive. Thus, the weak solutions pictured in Fig. 2 are proposed, each built

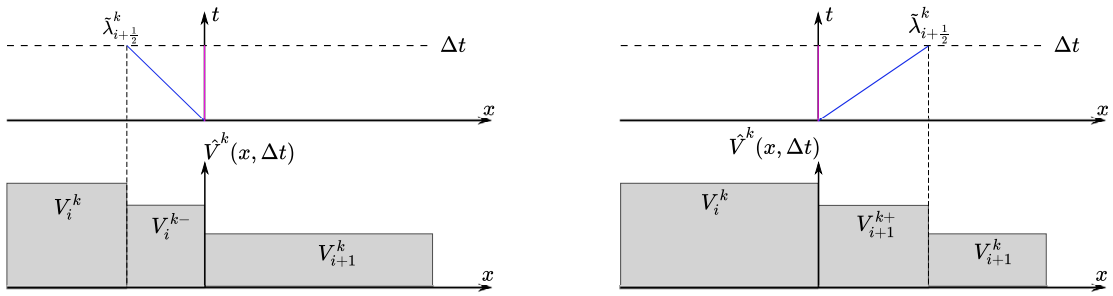

Fig. 2. Piecewise solution for the decoupled primitive variable $\hat{V}^k$, involving an inner constant state bound by a stationary contact wave at $x = x_{i+\frac{1}{2}}$ and by a wave of speed $\tilde{\lambda}_k$.

from a different piecewise reconstruction of the approximate solution for a characteristic variable V^k with a wave of speed $\tilde{\lambda}_k < 0$ (left) and $\tilde{\lambda}_k > 0$ (right):

$$\hat{V}^k(x',\Delta t) = \begin{cases} V_i^k & if \quad x' < \tilde{\lambda}_k \Delta t \\ V_i^{k-} & if \quad \tilde{\lambda}_k \Delta t < x' < 0 \\ V_{i+1}^k & if \quad x' > 0 \end{cases} \qquad if \quad \tilde{\lambda}_k < 0, \tag{41}$$

$$\hat{V}^k(x',\Delta t) = \begin{cases} V_i^k & if \quad x' < 0 \\ V_{i+1}^{k+} & if \quad 0 < x' < \tilde{\lambda}_k \Delta t \\ V_{i+1}^k & if \quad x' > \tilde{\lambda}_k \Delta t \end{cases} \qquad if \quad \tilde{\lambda}_k > 0. \tag{42}$$

The intermediate states can be found integrating in their respective domains. If $\tilde{\lambda}_k < 0$, then the state V_i^{k-} bound between $[\tilde{\lambda}_k \Delta t, 0]$, can be written as:

$$V_i^{k-} = \int_{\tilde{\lambda}_k \Delta t}^{0} V^k(x',\Delta t)dx = \frac{\tilde{\lambda}_k V_i^k + \tilde{\lambda}_k \left(V_{i+1}^k - V_i^k\right) - \tilde{\beta}_k}{\tilde{\lambda}_k} = V_i^k + \delta V_{i+\frac{1}{2}}^k - \frac{\tilde{\beta}_k}{\tilde{\lambda}_k}. \tag{43}$$

Likewise, the state V_{i+1}^{k+} bound between $[0, \tilde{\lambda}_k \Delta t]$ is given by:

$$V_{i+1}^{k+} = \int_{0}^{\tilde{\lambda}_k \Delta t} V^k(x',\Delta t)dx = \frac{\tilde{\lambda}_k V_{i+1}^k - \tilde{\lambda}_k \left(V_{i+1}^k - V_i^k\right) + \tilde{\beta}_k}{\tilde{\lambda}_k} = V_{i+1}^k - \delta V_{i+\frac{1}{2}}^k + \frac{\tilde{\beta}_k}{\tilde{\lambda}_k}. \tag{44}$$

where the terms $\delta V_{i+\frac{1}{2}}^k$ are kept in order to define the vector of wave strengths, which represent the difference in the primitive variables across the shock that the waves represent

$$\tilde{\mathbf{A}}_{i+\frac{1}{2}} = \delta \mathbf{V}_{i+\frac{1}{2}} = \tilde{\mathbf{P}}^{-1} \delta \mathbf{U}_{i+\frac{1}{2}} = (\tilde{\alpha}_1, \tilde{\alpha}_2)^T_{i+\frac{1}{2}} \tag{45}$$

In general, the average states at the cell wall can be written, according to the sign of the corresponding eigenvalue:

$$V_i^{k-} = \begin{cases} V_i^k & if \quad \tilde{\lambda}_k > 0 \\ V_i^k + \tilde{\theta}_k \delta V_{i+\frac{1}{2}}^k & if \quad \tilde{\lambda}_k < 0 \end{cases} \quad , \quad V_{i+1}^{k+} = \begin{cases} V_{i+1}^k - \tilde{\theta}_k \delta V_{i+\frac{1}{2}}^k & if \quad \tilde{\lambda}_k > 0 \\ V_{i+1}^k & if \quad \tilde{\lambda}_k < 0 \end{cases} \tag{46}$$

where

$$\tilde{\theta}_k = 1 - \frac{\tilde{\beta}_k}{\tilde{\lambda}_k \tilde{\alpha}_k}. \tag{47}$$

Expression (46) can be written in a more condensed form defining the positive and negative parts of the eigenvalue $\tilde{\lambda}_k^-$ and $\tilde{\lambda}_k^+$:

$$\tilde{\lambda}_k^{\pm} = \frac{1}{2}(\tilde{\lambda}_k \pm |\tilde{\lambda}_k|), \tag{48}$$

so the first is zero when $\tilde{\lambda}_k$ is positive and equal to $\tilde{\lambda}_k$ when it is negative. The opposite definition holds for $\tilde{\lambda}_k^+$. Then:

$$V_i^{k,-} = V_i^k + \left(\frac{\tilde{\lambda}^-}{\tilde{\lambda}}\right)_k \tilde{\theta}_k \delta V_{i+\frac{1}{2}}^k, \quad V_{i+1}^{k,+} = V_{i+1}^k - \left(\frac{\tilde{\lambda}^+}{\tilde{\lambda}}\right)_k \tilde{\theta}_k \delta V_{i+\frac{1}{2}}^k, \tag{49}$$

which allows grouping in matrix form

$$\mathbf{V}_i^- = \mathbf{V}_i + \tilde{\mathbf{\Lambda}}^{-1} \tilde{\mathbf{\Lambda}}^- \tilde{\mathbf{\Theta}} \delta \mathbf{V}_{i+\frac{1}{2}}, \qquad \mathbf{V}_{i+1}^+ = \mathbf{V}_{i+1} - \tilde{\mathbf{\Lambda}}^{-1} \tilde{\mathbf{\Lambda}}^+ \tilde{\mathbf{\Theta}} \delta \mathbf{V}_{i+\frac{1}{2}}, \tag{50}$$

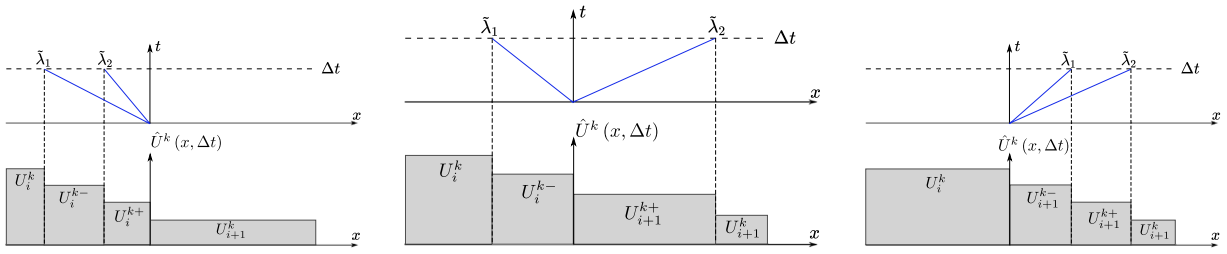

Fig. 3. Approximate solution $\hat{\mathbf{U}}(x,\Delta t)$ in the subcritical (center) and supercritical (left/right) cases. In the former case, the solution consists of two inner constant states, $\mathbf{U}_i^-$ and $\mathbf{U}_{i+1}^+$ given by (52), separated by a contact wave at $x = x_{i+\frac{1}{2}}$. In the latter cases, the solution consists of two inner constant states, $\mathbf{U}_i^-$ and $\mathbf{U}_i^+$ when $\tilde{\lambda}_2 < 0$, and $\mathbf{U}_{i+1}^-$ and $\mathbf{U}_{i+1}^+$ when $\tilde{\lambda}_1 > 0$.

where $\tilde{\boldsymbol{\Theta}}$ is a diagonal matrix with θ's in the main diagonal

$$\tilde{\boldsymbol{\Theta}}_{i+\frac{1}{2}} = \begin{pmatrix} \tilde{\theta}_1 & 0 \\ 0 & \tilde{\theta}_2 \end{pmatrix}_{i+\frac{1}{2}}. \tag{51}$$

Knowing the solution of the decoupled equations, it is now a matter of returning to the original conserved variables. The intermediate states $\mathbf{U}_i^-$ and $\mathbf{U}_{i+1}^+$ can be directly obtained by using $\tilde{\mathbf{P}}$ matrix. Vector solutions $\mathbf{U}_i^- = \tilde{\mathbf{P}}\mathbf{V}_i^-$ and $\mathbf{U}_{i+1}^+ = \tilde{\mathbf{P}}\mathbf{V}_{i+1}^+$ are recovered from (50) as follows

$$\begin{aligned} \mathbf{U}_i^- &= \mathbf{U}_i + (\tilde{\mathbf{P}}\tilde{\boldsymbol{\Lambda}}^{-1}\tilde{\boldsymbol{\Lambda}}^-\tilde{\boldsymbol{\Theta}}\tilde{\mathbf{P}}^{-1})_{i+\frac{1}{2}}\delta\mathbf{U}_{i+\frac{1}{2}} = \mathbf{U}_i + \sum_{\tilde{\lambda}^k<0}\left(\tilde{\alpha}\tilde{\theta}\tilde{\mathbf{e}}\right)_k, \\ \mathbf{U}_{i+1}^+ &= \mathbf{U}_{i+1} - (\tilde{\mathbf{P}}\tilde{\boldsymbol{\Lambda}}^{-1}\tilde{\boldsymbol{\Lambda}}^+\tilde{\boldsymbol{\Theta}}\tilde{\mathbf{P}}^{-1})_{i+\frac{1}{2}}\delta\mathbf{U}_{i+\frac{1}{2}} = \mathbf{U}_{i+1} - \sum_{\tilde{\lambda}^k>0}\left(\tilde{\alpha}\tilde{\theta}\tilde{\mathbf{e}}\right)_k. \end{aligned} \tag{52}$$

These two constant states at each side of the cell wall can be related using Eq. (31), where the Roe Jacobian is introduced as the constant and invertible Jacobian:

$$\mathbf{U}_{i+1}^+ - \mathbf{U}_i^- = \tilde{\mathbf{J}}_{i+\frac{1}{2}}^{-1}\bar{\mathbf{S}}_{i+\frac{1}{2}} = \tilde{\mathbf{H}}_{i+\frac{1}{2}} = -\frac{1}{\tilde{\lambda}_1\tilde{\lambda}_2}\begin{pmatrix} \bar{S}_{i+\frac{1}{2}} \\ 0 \end{pmatrix}. \tag{53}$$

where $\tilde{\mathbf{H}}$ has been defined in general in (33). The resulting self-similar solution of the IVP in (20) is depicted in Fig. 3 in all cases.

Since this piecewise description of the solution is based on shocks and steady waves, it is possible to utilize the Rankine–Hugoniot conditions:

$$\mathbf{F}_{i+1} - \mathbf{F}_{i+1}^+ = \tilde{\lambda}_2(\mathbf{U}_{i+1} - \mathbf{U}_{i+1}^+), \qquad \mathbf{F}_i^- - \mathbf{F}_i = \tilde{\lambda}_1(\mathbf{U}_i^- - \mathbf{U}_i) \tag{54}$$

and using the expressions for the intermediate states given in (53):

$$\mathbf{F}_{i+\frac{1}{2}}^+ = \mathbf{F}_{i+1}^+ = \mathbf{F}_{i+1} - \sum_{\tilde{\lambda}_k>0}[\tilde{\lambda}\tilde{\alpha}\tilde{\theta}\tilde{\mathbf{e}}]^k, \qquad \mathbf{F}_{i+\frac{1}{2}}^- = \mathbf{F}_i^- = \mathbf{F}_i + \sum_{\tilde{\lambda}_k<0}[\tilde{\lambda}\tilde{\alpha}\tilde{\theta}\tilde{\mathbf{e}}]^k. \tag{55}$$

which is also appropiate in the supercritical cases.

The process is now completed, as the knowledge of the inter-cell fluxes at the cell wall given in (55) allows to substitute into (11), Godunov's Scheme, with the following property:

$$\mathbf{F}_{i+1}^+ - \mathbf{F}_i^- = \bar{\mathbf{S}}_{i+\frac{1}{2}}. \tag{56}$$

3.4. The HLLS solver

HLL methods also propose a piecewise weak solution constructed from constant approximate inter-cell states bound by the eigenvalues of the Jacobian. The key difference with the Roe method is that, rather than choosing an approximate linearization of the Jacobian that yields certain eigenvalues $\tilde{\lambda}$ associated with positive and negative contributions to the flux, the basic HLL method considers two chosen waves, making the method simpler. An extension to the HLL, henceforth the HLLS method, includes a steady contact wave at the discontinuity and accounts for problems with source terms. The choice of waves, $\sigma_L < \sigma_R$ is, of course, very important to ensure good results, and will be discussed in Section 5.

Consider first the subcritical case $\sigma_L < 0 < \sigma_R$. Then, a weak solution pictured in Fig. 4 is suggested. In order to find the fluxes at the discontinuity at $x = x_{i+\frac{1}{2}}$, the weak solution $\hat{\mathbf{U}}(x',\Delta t)$ is integrated over the control volume $[\sigma_L\Delta t, \sigma_R\Delta t]$:

$$\int_{\sigma_L\Delta t}^{\sigma_R\Delta t}\hat{\mathbf{U}}(x,\Delta t)dx = \frac{-\sigma_L\mathbf{U}_i^- + \sigma_R\mathbf{U}_{i+1}^+}{\sigma_R - \sigma_L}, \tag{57}$$

which in combination with the integral Eq. (22), leads to

$$-\sigma_L\mathbf{U}_i^- + \sigma_R\mathbf{U}_{i+1}^+ + \sigma_L\mathbf{U}_i - \sigma_R\mathbf{U}_{i+1} + (\mathbf{F}_{i+1} - \mathbf{F}_i - \bar{\mathbf{S}}_{i+\frac{1}{2}}) = 0. \tag{58}$$

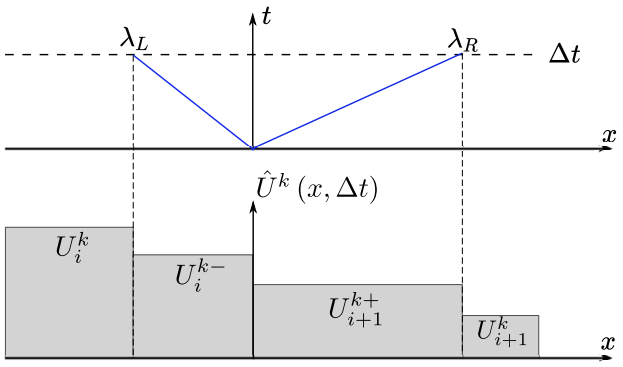

Fig. 4. Piecewise solution $\hat{\mathbf{U}}(x,\Delta t)$ in the subcritical case. The solution assumes of two inner constant states, $\mathbf{U}_i^-$ and $\mathbf{U}_{i+1}^+$ separated by a contact wave at $x=0$.

Another equation is necessary in order to solve for states $\mathbf{U}_{i+1}^+$ and $\mathbf{U}_i^-$. Of course these two are related by the $\bar{\mathbf{H}}$ vector first presented in (33).

$$\mathbf{U}_{i+1}^+ - \mathbf{U}_i^- = \bar{\mathbf{H}}_{i+\frac{1}{2}} = \left(\bar{\mathbf{J}}^{-1}\bar{\mathbf{S}}\right)_{i+\frac{1}{2}}. \tag{59}$$

Thus, assuming that $\bar{\mathbf{H}}$ is known, substitution of (59) into (58), allows to write the intermediate states:

$$\mathbf{U}_{i+1}^+ = \frac{\sigma_R\mathbf{U}_{i+1} - \sigma_L\mathbf{U}_i - \mathbf{F}_{i+1} + \mathbf{F}_i + \bar{\mathbf{S}}_{i+1/2} - \sigma_L\bar{\mathbf{H}}_{i+1/2}}{\sigma_R - \sigma_L} = \mathbf{U}^\star{}_{i+1/2} + \frac{\bar{\mathbf{S}}_{i+1/2} - \sigma_L\bar{\mathbf{H}}_{i+1/2}}{\sigma_R - \sigma_L}, \tag{60}$$

$$\mathbf{U}_i^- = \frac{\sigma_R\mathbf{U}_{i+1} - \sigma_L\mathbf{U}_i - \mathbf{F}_{i+F1} + \mathbf{F}_i + \bar{\mathbf{S}}_{i+1/2} - \sigma_R\bar{\mathbf{H}}_{i+1/2}}{\sigma_R - \sigma_L} = \mathbf{U}^\star{}_{i+1/2} + \frac{\bar{\mathbf{S}}_{i+1/2} - \sigma_R\bar{\mathbf{H}}_{i+1/2}}{\sigma_R - \sigma_L}. \tag{61}$$

where $\mathbf{U}^\star{}_{i+\frac{1}{2}}$ is the approximate state at the inter-cell wall in the homogeneous case, which in the context of the HLLS method, can be written:

$$\mathbf{U}^\star = \frac{\sigma_R\mathbf{U}_{i+1} - \sigma_L\mathbf{U}_i - \mathbf{F}_{i+1} + \mathbf{F}_i}{\sigma_R - \sigma_L}. \tag{62}$$

Knowing the inner states, the fluxes can be obtained by using the Rankine–Hugoniot conditions:

$$\mathbf{F}_{i+1} - \mathbf{F}_{i+1}^+ = \sigma_R(\mathbf{U}_{i+1} - \mathbf{U}_{i+1}^+), \qquad \mathbf{F}_i^- - \mathbf{F}_i = \sigma_L(\mathbf{U}_i^- - \mathbf{U}_i). \tag{63}$$

And therefore, in the subcritical regime, the fluxes needed to update following the Godunov method in (11) are:

$$\mathbf{F}_{i+\frac{1}{2}}^+ = \mathbf{F}_{i+1}^+ = \frac{\sigma_R\mathbf{F}_i - \sigma_L\mathbf{F}_{i+1} - \sigma_L\sigma_R(\mathbf{U}_{i+1} - \mathbf{U}_i) + \sigma_R(\bar{\mathbf{S}}_{i+1/2} - \sigma_L\bar{\mathbf{H}}_{i+1/2})}{\sigma_R - \sigma_L}, \tag{64}$$

$$\mathbf{F}_{i+\frac{1}{2}}^- = \mathbf{F}_i^- = \frac{\sigma_R\mathbf{F}_i - \sigma_L\mathbf{F}_{i+1} - \sigma_L\sigma_R(\mathbf{U}_{i+1} - \mathbf{U}_i) + \sigma_L(\bar{\mathbf{S}}_{i+1/2} - \sigma_R\bar{\mathbf{H}}_{i+1/2})}{\sigma_R - \sigma_L}. \tag{65}$$

The expressions for the inter-cell fluxes for the supercritical cases can be found in Appendix B.

In contrast to the HLL method, the need for an extra equation that forces the appearance of the $\bar{\mathbf{H}}_{i+\frac{1}{2}}$ can be problematic in certain situations, since an approximate Jacobian to compute $\bar{\mathbf{H}}$ needs to be chosen. Previous work in [25] universally chooses the Roe approximation $\tilde{\mathbf{H}}$ but this is not necessarily the best choice. Section 5 will detail why.

4. Entropy fix for transcritical rarefactions in the ARoe solver

The previous section dealt with finding weak solutions to the 1D SWE. However, not all weak solutions may correspond to physically meaningful solutions. Therefore, a series of corrections, generally referred to as entropy corrections are necessary to ensure the solution is the desired, physically correct solution [11,47,48]. These corrections were originally implemented for the Euler equations to ensure that weak solutions satisfied the principle of maximum entropy production in gas dynamics [10]. In the context of transcritical rarefaction, this is classically known as *the Entropy Fix*.

4.1. Homogeneous case

Consider first the homogeneous case in which the local RP is given by (8). Fig. 5 pictures a solution with a transcritical rarefaction (top) and its Roe-approximated counterpart $\hat{\mathbf{U}}(x',\Delta t)$ (bottom).

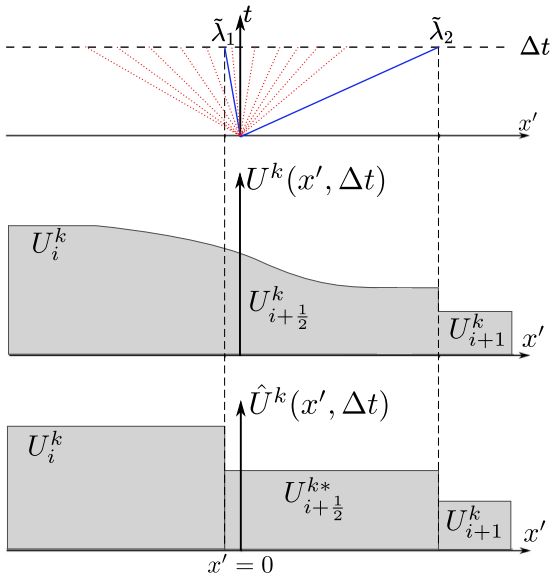

Fig. 5. Analytical $\mathbf{U}(x,t)$ and approximate solution $\hat{\mathbf{U}}(x,t)$ proposed by the ARoe method in the homogeneous case with a left transcritical rarefaction. The central state $\mathbf{U}^\star$ barely propagates in the left direction.

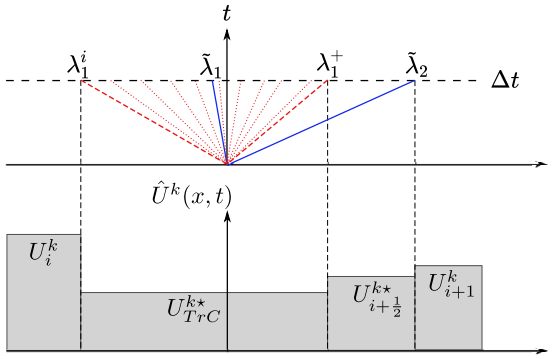

Fig. 6. New average solution in the homogeneous case with a transcritical rarefaction to the left. A new average state, $\mathbf{U}_{TrC}^\star$ is identified bounded by the rarefaction.

The central state $\mathbf{U}^\star$, given by:

$$\mathbf{U}_{i+\frac{1}{2}}^\star = \mathbf{U}_i + \sum_{\tilde{\lambda}^k<0} (\tilde{\alpha}\tilde{\mathbf{e}})_{i+\frac{1}{2}}^k = \mathbf{U}_{i+1} - \sum_{\tilde{\lambda}^k>0} (\tilde{\alpha}\tilde{\mathbf{e}})_{i+\frac{1}{2}}^k \tag{66}$$

barely propagates in the left directions respectively. Following Godunov's method in (11), the solution of the local RP is evolved for a time equal to the time step and the resulting solution is cell-averaged obtaining the piecewise solution at the new time level. However, in the case of a transcritical rarefaction, one of the Roe-averaged waves $\tilde{\lambda}_k$ does not represent the correct propagation of information carried by the rarefaction, as shown in Fig. 5, and thus the averaging is inaccurate.

Fig. 6 shows how the transcritical rarefaction, defined between λ_1^i and $\lambda_1^\star$, where:

$$\lambda_1^i = \lambda_1(\mathbf{U}_i) = u_i - \sqrt{g h_i} \qquad \text{and} \qquad \lambda_1^\star = \lambda_1(\mathbf{U}_{i+\frac{1}{2}}^\star) = u_{i+\frac{1}{2}}^\star - \sqrt{g h_{i+\frac{1}{2}}^\star}, \tag{67}$$

and fulfilling

$$\lambda_1^i < 0 < \lambda_1^\star, \tag{68}$$

can be substituted by the following transcritical average solution:

$$\mathbf{U}_{TrC}^\star = \frac{1}{\left(\lambda_1^\star - \lambda_1^i\right)\Delta t} \int_{\lambda_1^i \Delta t}^{\lambda_1^\star \Delta t} \mathbf{U}(x, \Delta t) dx, \tag{69}$$

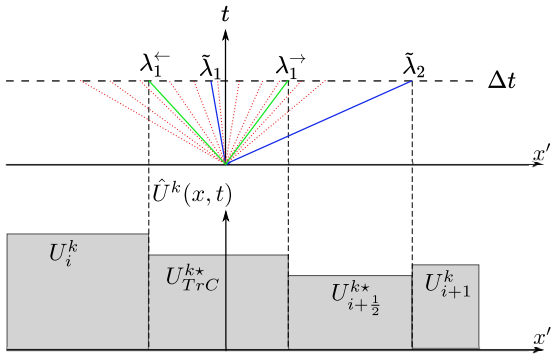

Fig. 7. New average solution in the homogeneous case with a transcritical rarefaction to the left. The split waves $\lambda_k^{\leftarrow}$, $\lambda_k^{\rightarrow}$ allow to compute the new central state as a linear combination.

where $\mathbf{U}^{\star}_{TrC}$ is a constant value that approximates the solution inside the rarefaction, bound by waves $\lambda_1^{\star}$ and λ_1^i, as can be seen in Fig. 6 at time $t^n + \Delta t$. This is usually tackled by the Harten–Hyman entropy fix [10], which splits the troublesome $\tilde{\lambda}_1$ into two wave contributions. The goal piecewise solution is represented in Fig. 7.

Integrating the approximate solution $\hat{\mathbf{U}}$ shown in Fig. 5 in the control volume given by the limits of the rarefaction fan (in red) $[\lambda_1^i \Delta t, \lambda_1^{\star} \Delta t]$ volume yields the average central state:

$$\mathbf{U}^{\star}_{TrC} = \frac{(\tilde{\lambda}_1 - \lambda_1^i)\mathbf{U}_i + (\lambda_1^{\star} - \tilde{\lambda}_1)\mathbf{U}^{\star}_{i+1/2}}{\lambda_1^{\star} - \lambda_1^i}. \tag{70}$$

Then, subtracting $\mathbf{U}_i$ from both sides of the equation:

$$\left(\mathbf{U}^{\star}_{TrC} - \mathbf{U}_i\right) = \frac{\lambda_1^{\star} - \tilde{\lambda}_1}{\lambda_1^{\star} - \lambda_1^i}\left(\mathbf{U}^{\star}_{i+\frac{1}{2}} - \mathbf{U}_i\right). \tag{71}$$

and then, if the $\tilde{\lambda}_1$ wave is treated like a shock, the Rankine–Hugoniot condition can be applied to it in order to obtain the flux difference across it:

$$\mathbf{F}^{\star}_{TrC} - \mathbf{F}_i = \lambda_1^i\left(\mathbf{U}^{\star}_{TrC} - \mathbf{U}_i\right) = \lambda_1^i \frac{\lambda_1^{\star} - \tilde{\lambda}_1}{\lambda_1^{\star} - \lambda_1^i}\left(\mathbf{U}^{\star}_{i+\frac{1}{2}} - \mathbf{U}_i\right). \tag{72}$$

Therefore, the flux across the cell wall is obtained:

$$\mathbf{F}_{i+\frac{1}{2}} = \mathbf{F}^{\star}_{TrC} = \mathbf{F}_i + \lambda_1^i \frac{\lambda_1^{\star} - \tilde{\lambda}_1}{\lambda_1^{\star} - \lambda_1^i}\tilde{\alpha}_1 \tilde{\mathbf{e}}^{\mathbf{1}} = \mathbf{F}_i + \lambda_1^{\leftarrow}\tilde{\alpha}_1 \tilde{\mathbf{e}}^{\mathbf{1}} \tag{73}$$

by using the newly defined:

$$\lambda_1^{\leftarrow} = \lambda_1^i \frac{\lambda_1^{+} - \tilde{\lambda}_1}{\lambda_1^{\star} - \lambda_1^i}. \tag{74}$$

This new wave can be thought of the part of the information traveling upstream with the transcritical rarefaction. Likewise, using the same reasoning, the celerity of the wave traveling downstream can be written as:

$$\lambda_1^{\rightarrow} = \lambda_1^{\star} \frac{\tilde{\lambda}_1 - \lambda_1^i}{\lambda_1^{\star} - \lambda_1^i}. \tag{75}$$

Note that these waves fulfill the property $\lambda_1^{\rightarrow} + \lambda_1^{\leftarrow} = \tilde{\lambda}_1$, as expected from the splitting. Fig. 7 shows the resulting approximate solution, with the central state $\mathbf{U}^{\star}_{TrC}$ bounded by the split waves.

In the case of a right transcritical rarefaction, bounded by $\lambda_2^{\star} = u^{\star}_{i+\frac{1}{2}} + \sqrt{g h^{\star}_{i+\frac{1}{2}}}$ and $\lambda_2^{i+1} = u_{i+1} + \sqrt{g h_{i+1}}$, the same process can be followed, arriving to the inter-cell flux given by:

$$\mathbf{F}_{i+\frac{1}{2}} = \mathbf{F}^{\star}_{\mathbf{TrC}} = \mathbf{F}_{i+1} - \lambda_2^{i+1} \frac{\tilde{\lambda}_2 - \lambda_2^{\star}}{\lambda_2^{i+1} - \lambda_2^{\star}}\tilde{\alpha}_2 \tilde{\mathbf{e}}^{\mathbf{2}} = \mathbf{F}_{i+1} - \lambda_2^{\rightarrow}\tilde{\alpha}_2 \tilde{\mathbf{e}}^{\mathbf{2}}, \tag{76}$$

where, again, two new waves appear in order to split the contribution of the rarefaction:

$$\lambda_2^{\rightarrow} = \lambda_2^{i+1} \frac{\tilde{\lambda}_2 - \lambda_2^{\star}}{\lambda_2^{i+1} - \lambda_2^{\star}}, \quad \lambda_2^{\leftarrow} = \lambda_2^{\star} \frac{\lambda_2^{i+1} - \tilde{\lambda}_2}{\lambda_2^{i+1} - \lambda_2^{\star}}. \tag{77}$$

fulfilling $\lambda_2^{\rightarrow} + \lambda_2^{\leftarrow} = \tilde{\lambda}_2$.

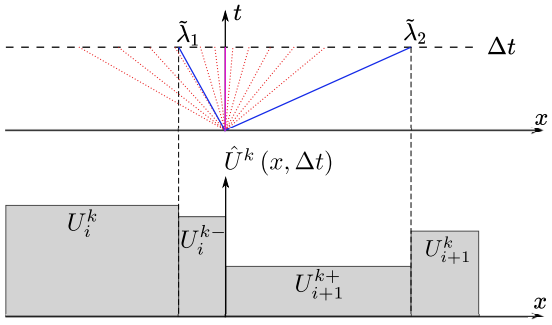

Fig. 8. Approximate solution $\hat{\mathbf{U}}(x,t)$ with a transcritical rarefaction to the left using the Roe averages $\tilde{\lambda}_k$. The central state $\mathbf{U}_i^-$ (left) barely propagate.

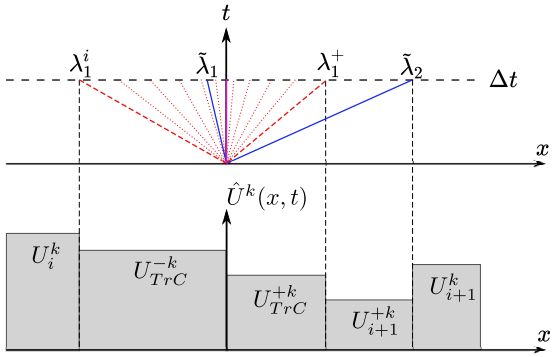

Fig. 9. Approximate solution $\hat{\mathbf{U}}(x,t)$ with a transcritical rarefaction to the left . Two new average states, $\mathbf{U}_{TrC}^-$ and $\mathbf{U}_{TrC}^-$ are identified bounded by the rarefaction.

4.2. Inhomogeneous case

Now the channel bed is added to the SWE model as a source term. Assume it is appropriately linearized at each inter-cell wall so its approximate solution resembles Fig. 8, with the source term acting at $x' = 0$.

The approximate solution is constructed from central states $\mathbf{U}_i^-$ and $\mathbf{U}_{i+1}^+$ as defined in (52). However, only one of the these central states can be calculated normally, $\mathbf{U}_{i+1}^+$ in this case:

$$\mathbf{U}_{i+1}^+ = \mathbf{U}_{i+1} - \tilde{\alpha}_2\theta_2\tilde{\mathbf{e}}_2. \tag{78}$$

It is assumed for now that the rarefaction is bounded between λ_1^i and λ_1^+, where:

$$\lambda_1^i = \lambda_1(\mathbf{U}_i) = u_i - \sqrt{gh_i} \qquad \text{and} \qquad \lambda_1^+ = \lambda_1(\mathbf{U}_{i+1}^+) = u_{i+1}^+ - \sqrt{gh_{i+1}^+}, \tag{79}$$

with:

$$\lambda_1^i < 0 < \lambda_1^+. \tag{80}$$

making it transcritical. Unlike the homogeneous case, the rarefaction is now represented by two new averaged states separated by the contact wave at $x' = 0$ (see Fig. 9), whose expressions are given by the following average solutions:

$$\mathbf{U}_{TrC}^- = -\frac{1}{\lambda_1^i \Delta t}\int_{\lambda_1^i\Delta t}^{0} \mathbf{U}(x',\Delta t)dx, \quad \mathbf{U}_{TrC}^+ = \frac{1}{\lambda_1^+\Delta t}\int_0^{\lambda_1^+\Delta t} \mathbf{U}(x',\Delta t)dx, \tag{81}$$

where $\mathbf{U}_{TrC}^{\pm}$ are constant inner states defined in the rarefaction region at time $t^n + \Delta t$ and separated by the inter-cell wall. It is still desirable to be able to compute the inter-cell fluxes as linear combinations of wave contributions as in (52). Again, the troublesome $\tilde{\lambda}_1$ needs to be split into two wave contributions that can accomplish this, given that two new intermediate states have been generated, as shown in Fig. 10. By integrating (22) in the control volume $[\lambda_1^i\Delta t, \tilde{\lambda}_2]$, a consistency equation relating $\mathbf{U}_{TrC}^-$ and $\mathbf{U}_{TrC}^+$ can be found:

$$-\lambda_1^i\mathbf{U}_{TrC}^- + \lambda_1^+\mathbf{U}_{TrC}^+ + (\tilde{\lambda}_2 - \lambda_1^+)\mathbf{U}_{i+1}^+ + \lambda_1^i\mathbf{U}_i - \tilde{\lambda}_2\mathbf{U}_{i+1} + (\mathbf{F}_{i+1} - \mathbf{F}_i - \bar{\mathbf{S}}_{i+\frac{1}{2}}) = 0. \tag{82}$$

While in the homogeneous case it was already possible to find the intermediate state, the fact that there are two unknown intermediates makes the inhomogeneous case need another equation that relates them. We suggest using the approximated

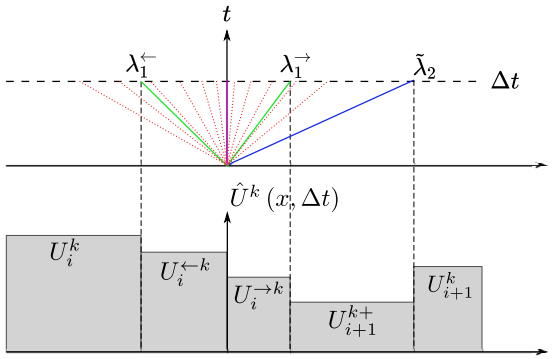

Fig. 10. New wave schemes resulting from applying a wave splitting method on the transcritical wave. In green, the new averaged waves that are used in the calculations. (For interpretation of the references to color in this figure legend, the reader is referred to the web version of this article.)

relation (53), where the inner states across the discontinuity are related through Roe's linearized Jacobian. Thus, the difference is approximated to:

$$\left(\mathbf{U}_{TrC}^{+} - \mathbf{U}_{TrC}^{-}\right) = \tilde{\mathbf{J}}^{-1}\tilde{\mathbf{S}}_{i+\frac{1}{2}} = \tilde{\mathbf{H}} = \frac{-1}{\tilde{\lambda}_1\tilde{\lambda}_2}\begin{pmatrix}\bar{S}_{i+\frac{1}{2}}\\ 0\end{pmatrix}. \tag{83}$$

where $\tilde{\mathbf{H}}$ in (33) has been approximated by $\tilde{\mathbf{H}}$, that is, Roe's linearization has been chosen in order to keep consistent with the scheme. With this expression, it is possible to substitute out one of the unknown states and solve for them, finding:

$$\mathbf{U}_{TrC}^{+} = \frac{\tilde{\lambda}_2\mathbf{U}_{i+1} - \lambda_1^i\mathbf{U}_i - (\tilde{\lambda}_2 - \lambda_1^+)\mathbf{U}_{i+1}^+ + \mathbf{F}_i - \mathbf{F}_{i+1} + \bar{\mathbf{S}}_{i+1/2} - \lambda_1^i\tilde{\mathbf{H}}}{\lambda_1^+ - \lambda_1^i} \tag{84}$$

$$\mathbf{U}_{TrC}^{-} = \frac{\tilde{\lambda}_2\mathbf{U}_{i+1} - \lambda_1^i\mathbf{U}_i - (\tilde{\lambda}_2 - \lambda_1^+)\mathbf{U}_{i+1}^+ + \mathbf{F}_i - \mathbf{F}_{i+1} + \bar{\mathbf{S}}_{i+1/2} - \lambda_1^+\tilde{\mathbf{H}}}{\lambda_1^+ - \lambda_1^i}. \tag{85}$$

Further manipulation of these two expressions, using Eq. (26) to substitute out the flux terms, leads to expressing the inner states as:

$$\mathbf{U}_{TrC}^{+} = \frac{(\tilde{\lambda}_1 - \lambda_1^i)\mathbf{U}_i + (\lambda_1^+ - \tilde{\lambda}_1)\mathbf{U}_{i+1}^+}{\lambda_1^+ - \lambda_1^i} - \frac{\lambda_1^i}{\lambda_1^+ - \lambda_1^i}\tilde{\mathbf{H}} \tag{86}$$

$$\mathbf{U}_{TrC}^{-} = \frac{(\tilde{\lambda}_1 - \lambda_1^i)\mathbf{U}_i + (\lambda_1^+ - \tilde{\lambda}_1)\mathbf{U}_{i+1}^+}{\lambda_1^+ - \lambda_1^i} - \frac{\lambda_1^+}{\lambda_1^+ - \lambda_1^i}\tilde{\mathbf{H}} \tag{87}$$

meaning that the difference between the transcritical inner states and their neighboring average states can be expressed using known states such as $\mathbf{U}_{i+1}^+$ and $\mathbf{U}_i$

$$\mathbf{U}_{i+1}^{+} - \mathbf{U}_{TrC}^{+} = \frac{\tilde{\lambda}_1 - \lambda_1^+}{\lambda_1^+ - \lambda_1^i}(\mathbf{U}_{i+1}^+ - \mathbf{U}_i) + \frac{\lambda_1^i}{\lambda_1^+ - \lambda_1^i}\tilde{\mathbf{H}} \tag{88}$$

$$\mathbf{U}_{TrC}^{-} - \mathbf{U}_i = \frac{\lambda_1^+ - \tilde{\lambda}_1}{\lambda_1^+ - \lambda_1^i}(\mathbf{U}_{i+1}^+ - \mathbf{U}_i) - \frac{\lambda_1^+}{\lambda_1^+ - \lambda_1^i}\tilde{\mathbf{H}}. \tag{89}$$

By virtue of the Rankine–Hugoniot conditions and treating discontinuities λ_1^+ and λ_1^i as shocks, the fluxes corresponding to the transcritical states can be expressed as

$$\mathbf{F}_{i+1}^{+} - \mathbf{F}_{TrC}^{+} = \lambda_1^+(\mathbf{U}_{i+1}^+ - \mathbf{U}_{TrC}^+) \tag{90}$$

$$\mathbf{F}_{TrC}^{-} - \mathbf{F}_i = \lambda_1^i(\mathbf{U}_{TrC}^- - \mathbf{U}_i), \tag{91}$$

or, expanding the jumps into the wave strengths as it is done in the Roe method

$$\mathbf{F}_{TrC}^{+} = \mathbf{F}_{i+1}^{+} - \lambda_1^+\frac{(\tilde{\lambda}_1 - \lambda_1^+)}{\lambda_1^+ - \lambda_1^i}\left(\tilde{\alpha}_1 - \frac{\beta_1}{\tilde{\lambda}_1}\right)\tilde{\mathbf{e}}^{\mathbf{1}} - \frac{\lambda_1^+\lambda_1^i}{\lambda_1^+ - \lambda_1^i}\tilde{\mathbf{H}}_{i+\frac{1}{2}} \tag{92}$$

$$\mathbf{F}_{TrC}^{-} = \mathbf{F}_i + \lambda_1^i\frac{(\lambda_1^+ - \tilde{\lambda}_1)}{\lambda_1^+ - \lambda_1^i}\left(\tilde{\alpha}_1 - \frac{\beta_1}{\tilde{\lambda}_1}\right)\tilde{\mathbf{e}}^{\mathbf{1}} - \frac{\lambda_1^i\lambda_1^+}{\lambda_1^+ - \lambda_1^i}\tilde{\mathbf{H}}_{i+\frac{1}{2}}. \tag{93}$$

Precisely from these expressions, the new split waves are defined, along with the splitting of the source term

$$\lambda_1^{\rightarrow} = \lambda_1^+\frac{\tilde{\lambda}_1 - \lambda_1^i}{\lambda_1^+ - \lambda_1^i} \qquad \beta_1^{\rightarrow} = \frac{\lambda_1^+}{\tilde{\lambda}_1}\frac{\tilde{\lambda}_1 - \lambda_1^i}{\lambda_1^+ - \lambda_1^i}\beta_1 = \frac{\lambda_1^{\rightarrow}}{\tilde{\lambda}_1}\beta_1, \tag{94}$$

$$\lambda_1^{\leftarrow} = \lambda_1^i \frac{\lambda_1^+ - \tilde{\lambda}_1}{\lambda_1^+ - \lambda_1^i} \qquad \beta_1^{\leftarrow} = \frac{\lambda_1^i}{\tilde{\lambda}_1} \frac{\lambda_1^+ - \tilde{\lambda}_1}{\lambda_1^+ - \lambda_1^i} \beta_1 = \frac{\lambda_1^{\leftarrow}}{\tilde{\lambda}_1} \beta_1. \tag{95}$$

Of course, these fulfill $\lambda_1^{\leftarrow} + \lambda_1^{\rightarrow} = \tilde{\lambda}_1$ and $\beta_1^{\leftarrow} + \beta_1^{\rightarrow} = \tilde{\beta}_1$, as should be. Using the new waves, the fluxes can be rewritten:

$$\mathbf{F}_{TrC}^+ = \mathbf{F}_{i+1}^+ - \left(\lambda_1^{\rightarrow} \tilde{\alpha}_1 - \beta_1^{\rightarrow} \right) \tilde{\mathbf{e}}^{\mathbf{1}} - \frac{\lambda_1^+ \lambda_1^i}{\lambda_1^+ - \lambda_1^i} \tilde{\mathbf{H}}_{i+\frac{1}{2}} \tag{96}$$

$$\mathbf{F}_{TrC}^- = \mathbf{F}_i + \left(\lambda_1^{\leftarrow} \tilde{\alpha}_1 - \beta_1^{\leftarrow} \right) \tilde{\mathbf{e}}^{\mathbf{1}} - \frac{\lambda_1^i \lambda_1^+}{\lambda_1^+ - \lambda_1^i} \tilde{\mathbf{H}}_{i+\frac{1}{2}}. \tag{97}$$

where $\mathbf{F}_{i+1}^+$ can be calculated using the other wave $\tilde{\lambda}_2$. Then, all of the quantities involved in their calculation are known, and therefore these expressions can be implemented in the Riemann Solver in a manner that resembles the usual Roe implementations. Recalling the definition of $\tilde{\theta}_k$ in Eq. (47), the fluxes can be compactly written:

$$\mathbf{F}_{i+\frac{1}{2}}^+ = \mathbf{F}_{TrC}^+ = \mathbf{F}_{i+1} - \tilde{\lambda}_2 \tilde{\theta}_2 \tilde{\mathbf{e}}^{\mathbf{2}} - \lambda_1^{\rightarrow} \tilde{\theta}_1^{\rightarrow} \tilde{\mathbf{e}}^{\mathbf{1}} - \frac{\lambda_1^+ \lambda_1^i}{\lambda_1^+ - \lambda_1^i} \tilde{\mathbf{H}}_{i+\frac{1}{2}} \tag{98}$$

$$\mathbf{F}_{i+\frac{1}{2}}^- = \mathbf{F}_{TrC}^- = \mathbf{F}_i + \lambda_1^{\leftarrow} \tilde{\theta}_1^{\leftarrow} \tilde{\mathbf{e}}^{\mathbf{1}} - \frac{\lambda_1^i \lambda_1^+}{\lambda_1^+ - \lambda_1^i} \tilde{\mathbf{H}}_{i+\frac{1}{2}}, \tag{99}$$

having substituted:

$$\mathbf{F}_{i+1}^+ = \mathbf{F}\left(\mathbf{U}_{i+1}^+ \right) = \mathbf{F}_{i+1} - \tilde{\lambda}_2 \tilde{\theta}_2 \tilde{\mathbf{e}}^{\mathbf{2}}, \tag{100}$$

and

$$\theta_k^{\leftarrow} = 1 - \left(\frac{\beta_k^{\leftarrow}}{\lambda_k^{\leftarrow} \alpha_k} \right), \quad \theta_k^{\rightarrow} = 1 - \left(\frac{\beta_k^{\rightarrow}}{\lambda_k^{\rightarrow} \alpha_k} \right). \tag{101}$$

If the rarefaction is bounded between λ_2^- and λ_2^{i+1}, it is considered a right transcritical rarefaction, where:

$$\lambda_2^- = \lambda_2(\mathbf{U}_i^-) = u_i^- + \sqrt{g h_i^-} \qquad \text{and} \qquad \lambda_2^{i+1} = \lambda_2(\mathbf{U}_{i+1}) = u_{i+1} + \sqrt{g h_{i+1}}. \tag{102}$$

Then, the entropy fix requires computation of new waves $\lambda_2^{\rightarrow}$ and $\lambda_2^{\leftarrow}$, and source contributions $\beta^{\rightarrow}$ and $\beta^{\leftarrow}$. Their forms is given in Appendix C, along with the reasoning used to obtain them. Then, the fluxes are computed as:

$$\mathbf{F}_{i+\frac{1}{2}}^+ = \mathbf{F}_{TrC}^+ = \mathbf{F}_{i+1} - \left(\lambda_2^{\leftarrow} \tilde{\alpha}_2 - \beta_2^{\leftarrow} \right) \tilde{\mathbf{e}}^{\mathbf{2}} - \frac{\lambda_2^{i+1} \lambda_2^-}{\lambda_2^{i+1} - \lambda_2^-} \tilde{\mathbf{H}}_{i+\frac{1}{2}} \tag{103}$$

$$\mathbf{F}_{i+\frac{1}{2}}^- = \mathbf{F}_{TrC}^- = \mathbf{F}_i + \left(\tilde{\lambda}_1 \tilde{\alpha}_1 - \beta_1 \right) \tilde{\mathbf{e}}^{\mathbf{1}} - \left(\lambda_2^{\rightarrow} \tilde{\alpha}_2 - \beta_2^{\rightarrow} \right) \tilde{\mathbf{e}}^{\mathbf{2}} - \frac{\lambda_2^- \lambda_2^{i+1}}{\lambda_2^{i+1} - \lambda_2^-} \tilde{\mathbf{H}}_{i+\frac{1}{2}}, \tag{104}$$

with

$$\lambda_2^{\rightarrow} = \lambda_2^{i+1} \frac{\tilde{\lambda}_2 - \lambda_2^-}{\lambda_2^{i+1} - \lambda_2^-} \qquad \beta_2^{\rightarrow} = \frac{\lambda_2^{i+1}}{\tilde{\lambda}_2} \frac{\tilde{\lambda}_2 - \lambda_2^-}{\lambda_2^{i+1} - \lambda_2^-} \beta_2 = \frac{\lambda_2^{\rightarrow}}{\tilde{\lambda}_2} \beta_2 \tag{105}$$

$$\lambda_2^{\leftarrow} = \lambda_2^- \frac{\lambda_2^{i+1} - \tilde{\lambda}_2}{\lambda_2^{i+1} - \lambda_2^-} \qquad \beta_2^{\leftarrow} = \frac{\lambda_2^-}{\tilde{\lambda}_2} \frac{\lambda_2^{i+1} - \tilde{\lambda}_2}{\lambda_2^{i+1} - \lambda_2^-} \beta_2 = \frac{\lambda_2^{\leftarrow}}{\tilde{\lambda}_2} \beta_2. \tag{106}$$

4.3. Simplification of the ARoe entropy correction

A simplification of the entropy correction for the ARoe method is shown here, relating the results obtained in this Section with the Harten–Hyman entropy correction for homogeneous cases. Given a transcritical rarefaction to the left that fulfills (68), the following approximation to the bounding waves of the rarefaction is taken [17,48]:

$$\lambda_1(\mathbf{U}_{i+1}^+) \approx \lambda_1(\mathbf{U}_{i+1}) = \lambda_1^{i+1}, \tag{107}$$

which means that the approximate condition to identify a left transcritical rarefaction is

$$\lambda_1(\mathbf{U_i}) < 0 < \lambda_1(\mathbf{U}_{i+1}). \tag{108}$$

The same idea can be applied to a right transcritical rarefaction, where:

$$\lambda_2(\mathbf{U}^-) \approx \lambda_2(\mathbf{U_i}) = \lambda_2^i, \tag{109}$$

and so the condition to identify it will be:

$$\lambda_2(\mathbf{U_i}) < 0 < \lambda_2(\mathbf{U}_{i+1}). \tag{110}$$

In addition to changing the criteria to identify transcritical rarefactions, this approximation changes the method used to fix the limitations of the ARoe solver under transcritical flow conditions. The split waves defined by (94) and (105) can also be simplified by eliminating the evaluation of the averaged state, allowing its calculation from only the left and right initial states.

$$\lambda_1^{\rightarrow} \approx \lambda_1^{i+1} \frac{\tilde{\lambda}_1 - \lambda_1^i}{\lambda_1^{i+1} - \lambda_1^i} \qquad \lambda_1^{\leftarrow} \approx \lambda_1^i \frac{\lambda_1^{i+1} - \tilde{\lambda}_1}{\lambda_1^{i+1} - \lambda_1^i}. \tag{111}$$

$$\lambda_2^{\rightarrow} \approx \lambda_2^{i+1} \frac{\tilde{\lambda}_2 - \lambda_2^i}{\lambda_2^{i+1} - \lambda_2^i} \qquad \lambda_2^{\leftarrow} \approx \lambda_2^i \frac{\lambda_2^{i+1} - \tilde{\lambda}_2}{\lambda_2^{i+1} - \lambda_2^L} \tag{112}$$

The Entropy Fix has been derived here by investigating the solution of an IVP with a non trivial solution, unlike steady states where the initial conditions match the final solution. This is the case of the acceleration and deceleration of a subsonic flow over a bump [17] where sonic flow conditions are achieved at the highest elevation point. The exact numerical discrete solution at this point with $z_{i+1} = z_{max}$, yields $\mathrm{Fr}_{i+1} = 1$, with $z_i < z_{i+1}$, and with $\mathrm{Fr}_i < 1$.

The resulting eigenvalues are $\lambda_1^i < 0$ and $\lambda_1^{i+1} = 0$ which does not fulfill condition (108). However, in the transitory regime evolving towards the stationary case described, the entropy correction must ensure convergence to the exact solution in the sonic point. There, the RP evolves to $\lambda_i < 0$ and $\lambda_{i+1} = \epsilon$. When steady state is achieved, $\epsilon \to 0$ to ensure $\mathrm{Fr}_i < 1$ and $\mathrm{Fr}_{i+1} = 1$ and to achieve this exact convergence the entropy correction is necessary. This is done using:

$$\lambda_1^{\leftarrow}(\epsilon \to 0) = \tilde{\lambda}_1 \qquad \lambda_1^{\rightarrow}(\epsilon \to 0) = 0\,. \tag{113}$$

It must be noted too that in the limit $\epsilon = 0$, $\beta_1^{\rightarrow}$ must forcibly be zero, as the inner state $\mathbf{U}^{\rightarrow}$ has null length. It is related to the static solution ray $x/t = 0$ at the inter-cell wall, producing a discontinuity between its neighbors $\mathbf{U}^{\leftarrow}$ and $\mathbf{U}_{i+1}^{+}$. Thus, this approximate state cannot participate either on the left or on the right side of the solution and an exact splitting of the source term cannot be provided. Therefore, only if setting

$$\beta_1^{\leftarrow} = \bar{\beta}_1\,, \qquad \beta_1^{\rightarrow} = 0\,, \tag{114}$$

convergence to the exact sonic point or its preservation is ensured, as the balance of fluxes and source terms is exactly reproduced. Furthermore, due to the approximations (107) and (109), the $\tilde{\mathbf{H}}$ term present in the calculation of the inter-cell fluxes in (98) and (99) vanishes when $\epsilon \to 0$ at the critical point in the steady case. Following this reasoning, the expressions for the inter-cell fluxes in the steady case:

$$\mathbf{F}^{+}_{i+\frac{1}{2}} = \mathbf{F}^{+}_{TrC} = \mathbf{F}_{i+1} - \left(\tilde{\lambda}_2\tilde{\alpha}_2 - \beta_2\right) - \left(\lambda_1^{\rightarrow}\tilde{\alpha}_1\right) \tag{115}$$

$$\mathbf{F}^{-}_{i+\frac{1}{2}} = \mathbf{F}^{-}_{TrC} = \mathbf{F}_{i} - \left(\lambda_1^{\leftarrow}\tilde{\alpha}_1 - \beta_1\right), \tag{116}$$

for a left transcritical rarefaction and, equivalently:

$$\mathbf{F}^{+}_{i+\frac{1}{2}} = \mathbf{F}^{+}_{TrC} = \mathbf{F}_{i+1} - \left(\lambda_2^{\rightarrow}\tilde{\alpha}_2 - \beta_2\right) \tag{117}$$

$$\mathbf{F}^{-}_{i+\frac{1}{2}} = \mathbf{F}^{-}_{TrC} = \mathbf{F}_{i} + \left(\tilde{\lambda}_1\tilde{\alpha}_1 - \beta_1\right) + \left(\lambda_2^{\leftarrow}\tilde{\alpha}_2\right) \tag{118}$$

for a right transcritical rarefaction.

5. Choice of waves in the HLLS solver

When computing the HLLS numerical fluxes, the selection of estimates for the wave speeds is of utmost importance, as they can compromise the quality of the numerical results. The simplest of these, according to Davis [49], are provided by direct wave speed estimates providing minimum and maximum signal velocities:

$$\sigma_L = \min(u_i - c_i, u_{i+1} - c_{i+1}), \quad \sigma_R = \max(u_i + c_i, u_{i+1} + c_{i+1}). \tag{119}$$

In the context of gas dynamics, Einfeldt [50] combined the direct estimates in (119) with the Roe averages (36). This option can be applied to shallow flows by including in the selection the average values $\tilde{\lambda}_1 = \tilde{u} - \tilde{c}$ and $\tilde{\lambda}_2 = \tilde{u} + \tilde{c}$. An important criterion in the selection, is that the resulting solver must ensure positively conservative solutions [51], that is, positive reconstructions of the conserved variables must be provided when necessary. In the shallow water context, this property ensures positive values of water depth in all the regions of the weak solution. In [23], Toro provided estimates based on approximations to exact solutions for the homogeneous shallow water equations.

In [25] the wave speeds σ_L and σ_R were approximated using

$$\sigma_L = \begin{cases} \min(\widetilde{\lambda}_1, u_i - c_i, u_{i+1} - c_{i+1}) & \text{if } |\bar{S}_{i+\frac{1}{2}}| = 0 \\ \widetilde{\lambda}_1 & \text{if } |\bar{S}_{i+\frac{1}{2}}| \neq 0 \end{cases}$$
$$\sigma_R = \begin{cases} \max(\widetilde{\lambda}_2, u_i + c_i, u_{i+1} + c_{i+1}) & \text{if } |\bar{S}_{i+\frac{1}{2}}| = 0 \\ \widetilde{\lambda}_2 & \text{if } |\bar{S}_{i+\frac{1}{2}}| \neq 0 \end{cases} \tag{120}$$

where, if source terms present at the local Riemann problem, the Roe estimates are chosen directly. However, the forced use of Roe-averaged waves in (120) also leads to the usual problems of this method, such as the need for an entropy correction in transcritical rarefaction, underlined in Section 4. As a solution, this work proposes the following approach:

$$\sigma_L = \min(\tilde{\lambda}_1, u_i - c_i), \qquad \sigma_R = \max(\tilde{\lambda}_2, u_{i+1} + c_{i+1}) \tag{121}$$

any case. This proves to be an advantage, since values of $\tilde{\lambda} \approx 0$, present in transcritical rarefactions, are never chosen. Rarefactions are represented by the wave whose velocity is the greatest in absolute terms.

Regarding the choice of approximate Jacobian $\bar{\mathbf{J}}_{i+\frac{1}{2}}$, necessary to formulate the difference in states across the inter-cell wall in the form of vector $\bar{\mathbf{H}}$, it was previously [25] always chosen to be the Roe Jacobian $\tilde{\mathbf{J}}$. It was argued that the Roe average variables would be a better approximation to the real unknown intermediate values. Nevertheless, it is worth considering other options for several reasons:

- The Roe eigenvalues $\tilde{\lambda}_1$ and $\tilde{\lambda}_2$ may not coincide in sign with the chosen waves σ_L and σ_R.
- The Roe eigenvalues may provide inaccurate estimates of the wave celerities, specially in transcritical rarefactions.

As a result it seems that approximating $\det \bar{\mathbf{J}}_{i+\frac{1}{2}} = \sigma_L \lambda_R$ is also a reasonable approach. This selection has a consequence when managing steady solutions including critical points with $u_i = \sqrt{g h_i}$ and $\lambda_1^i = 0$, where it is possible to find cases with $\lambda_1^i < \tilde{\lambda}$. Under this conditions, $\det \bar{\mathbf{J}}_{i+\frac{1}{2}} = 0$ and the resulting solution does not represent the correct propagation of information, as in those cases where entropy corrections were required, and exact solutions with critical points cannot be reproduced. In order to avoid this problem the following selection for $\det \bar{\mathbf{J}}_{i+\frac{1}{2}}$ is proposed:

$$\det \bar{\mathbf{J}}_{i+\frac{1}{2}} = \begin{cases} \tilde{\lambda}_1 \tilde{\lambda}_2 & \text{if} \quad |u_i - c_i| < \varepsilon \quad \text{or} \quad |u_{i+1} + c_{i+1}| < \varepsilon \\ \sigma_L \lambda_R & \text{otherwise} \end{cases}, \tag{122}$$

where $\varepsilon = 10^{-10}$ is the numerical tolerance used in this work.

6. Numerical experiments

A series of numerical experiments are presented here to show the improvements of the corrections over the previous implementations of the ARoe and HLLS methods. The particular goals are to test whether the fully expanded entropy fix for the ARoe solver is in any way better than the approximated entropy fix, and to compare the different versions of the HLLS method, varying the choice of waves and of linearized Jacobian. To do so, the test cases have been selected in order to check the preservation of the well-balanced property in cases with non zero velocity, or because previous works were unable to find a satisfactory numerical solution.

First, the batch of classic Riemann Problem first presented by LeFloch and Thanh in [5] have been selected. They include a bed elevation discontinuity so the source term has influence in their exact solutions and, additionally, their analytical solution is known. Out of these Riemann Problems, the first (RP 1) will serve to test whether the corrections keep the well-balancedness of the schemes, while cases 6 and 7 (RP 6 and RP 7) include critical transitions.

Second, the methods have been tested by solving the steady flow over a bump in the bed elevation for three different configurations that produce different combinations of hydraulic regimes in the domain. The interest of this test case lies in the fact that the critical point has known location. If the flow undergoes a transition from subcritical to supercritical, it will take place exactly at the point where the bed elevation is maximum.

In using the ARoe method, the variations tested and compared in order to evaluate the validity of the entropy fix are:

- The ARoe solver without any entropy correction for the purpose of showing why it is necessary. This version is labeled **ARoe1**.
- The ARoe solver, with a simplified version of the entropy fix, laid out in Section 4.3. This version is labeled **ARoe2**.
- The ARoe solver, with the full entropy correction developed in this paper and presented in Section 4.2. This version is labeled **ARoe3**.

Additionally, three instances of the HLLS method will be used and compared in order to evaluate the choice of waves and of the linearized Jacobian for the method:

Table 1
Collection of Riemann problems used to test the ARoe solvers.

	h (m)		u (m/s)		z [m]	
	L	R	L	R	L	R
RP 1	1.0	1.223656	5.0	4.086116	0.0	0.2
RP 2	0.3	0.374728	2.2	2.088732	0.1	0.0
RP 3	1.0	2.0	3.0	0.5	0.2	0.0
RP 4	1.0	1.2	3.0	0.5	0.1	0.0
RP 5	0.2	0.5	4.0	1.5	0.0	0.1
RP 6	0.2	0.759049	5.0	1.341074	0.0	0.2
RP 7	1.0	0.8	2.0	4.0	0.1	0.0

Table 2
Order of convergence of the six different methods tested to solve RP 7.

	RP 7 $\mathcal{O}(L_1)$					
N	ARoe1	ARoe2	ARoe3	HLL1	HLL2	HLL3
100	0.4501	0.7220	0.8979	0.4501	1.0496	0.7791
200	0.2582	0.6990	0.7372	0.2582	1.0019	0.7267
400	0.2060	0.6427	0.8018	0.2060	0.9233	0.7112
800	0.1217	0.7144	0.7163	0.1217	0.9099	0.7942
1600	0.0864	0.7162	0.7497	0.0864	0.7988	0.7338
3200	0.0541	0.7218	0.7388	0.0541	0.7262	0.7188

- The HLLS solver with wave speed estimates reduced to the Roe-averaged eigenvalues chosen whenever there is source term contribution, as laid out in (120), and the determinant of the Jacobian is $\det \bar{\mathbf{J}}_{i+\frac{1}{2}} = \tilde{\lambda}_1 \tilde{\lambda}_2$. This version will be labeled **HLLS1**.
- The HLLS solver with wave speed estimates selected among the most negative and positive between the Roe averages and the eigenvalues evaluated in the cells neighboring the inter-cell wall, (121). The determinant of the linearized Jacobian is still $\det \bar{\mathbf{J}}_{i+\frac{1}{2}} = \tilde{\lambda}_1 \tilde{\lambda}_2$. This version will be labeled **HLL2**.
- The HLLS solver with wave speed estimates selected among the most negative and positive between the Roe averages and the eigenvalues evaluated in the cells neighboring the inter-cell wall, (121). The determinant of the linearized Jacobian is chosen to be $\det \bar{\mathbf{J}}_{i+\frac{1}{2}} = \sigma_L \sigma_R$, unless these are too close to zero, in which case the Roe-averaged waves are chosen, as seen in (122). This version will be labeled **HLL3**.

6.1. Riemann problems with exact solutions

The initial conditions of the RP selected from [5] are presented in Table 1, where L and R refer to the left and right side of the discontinuity respectively. A domain 2 m long centered at $x = 0$ m is chosen and discretized in N cells of varying Δx, in order to perform a convergence analysis.

The computations have been carried out with a global time-step selected as the lowest of all local time-steps, computed as $\delta t_i = \mathrm{CFL} \frac{\delta x_i}{\max_k \left(\tilde{\lambda}^k_{i\pm\frac{1}{2}} \right)}$, where $\tilde{\lambda}^k_{i+\frac{1}{2}}$ are the Roe-averaged eigenvalues evaluated at either wall of each cell, for the ARoe method or $\delta t_i = \mathrm{CFL} \frac{\delta x_i}{\max_k \left(\sigma^{L,R}_{i\pm\frac{1}{2}} \right)}$ for the HLLS method. A value of CFL = 0.95 is chosen to show the capabilities of the methods.

The numerical results are plotted in different colors for an evolved time $t = 0.1$ s in Figs. 11–13, along with the analytical solution in black. Additionally, the error computed with respect to the analytical solution using the L_1 norm is plotted for all cases in Figs. 14 and 15. (See Table 2).

RP 1 has as initial state the exact solution of the problem and, therefore, is used to ensure that the method is able to maintain equilibrium states in time in presence of a discontinuous bed step. As Fig. 11 shows, the evolved state at $t = 0.1$ s matches the exact solution of a steady contact wave between the equilibrium states and the first plot at 14 shows that the error is of the order of machine precision, confirming that all methods are well-balanced in the absence of transcritical rarefactions. RPs 2 to 5 further show that all methods behave as expected from previous results [17], with all methods performing equally well. This was to be expected in the ARoe method, as in the absence of transcritical rarefaction all three variations work in the same way. However, for the HLLS method, it proves that all the choices of wave speeds presented are right. The rate of convergence of all methods is found to be approximately of 1, as expected for first order methods (see Table 2). The particularities of the test cases, which are very dynamical and contain sharp discontinuities, produce the discrepancies in this number.

RP 6 is singled out because it contains a transition from supercritical to subcritical regime. When this occurs, a discontinuity in water surface elevation, known as a hydraulic jump, takes place. Hydraulic jumps dissipate energy and are known to cause numerical defects which in this case manifest as oscillations near the discontinuity. This is a well-known problem already discussed in depth in [52] caused by the fact that the hydraulic jump, taking place at an unknown position, must be represented in a discretized grid.

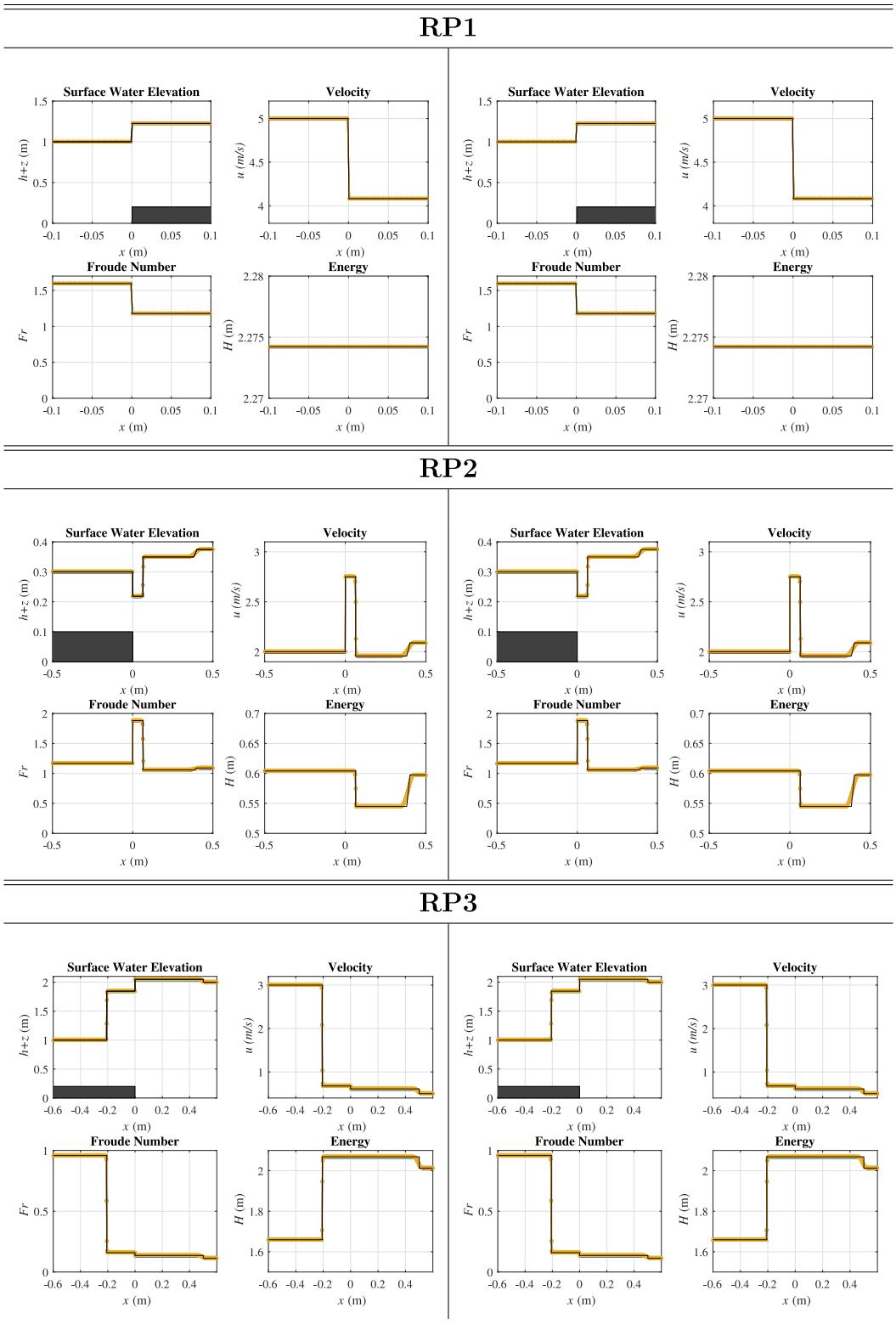

Fig. 11. RPs 1 trough 3 solved using the different versions of the ARoe solver (left) and of the HLLS solver (right). Methods ARoe1 and HLLS1 are plotted in blue, ARo2 and HLLS2 in red and ARoe3 and HLLS3 in yellow. (For interpretation of the references to color in this figure legend, the reader is referred to the web version of this article.)

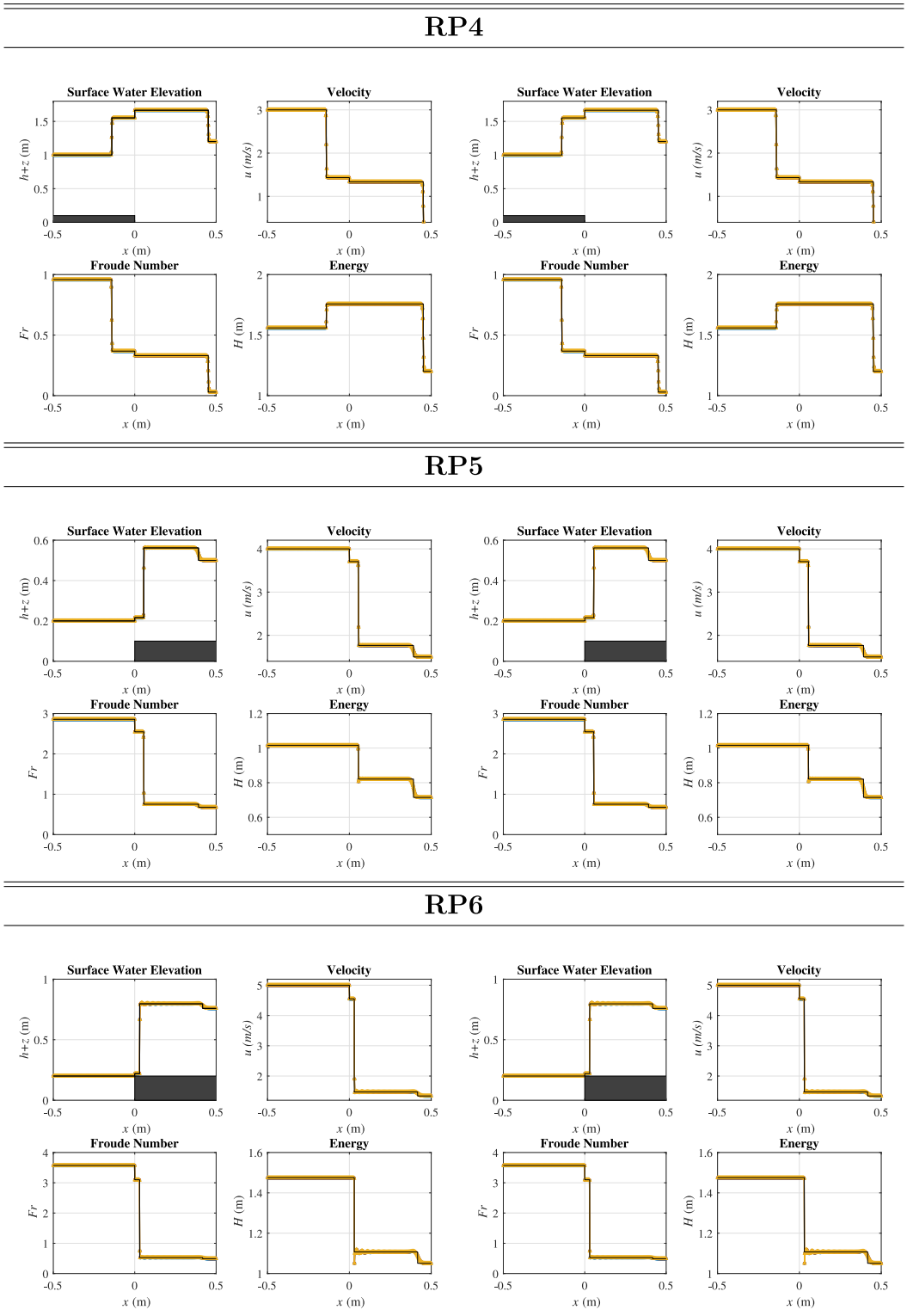

Fig. 12. RPs 4 trough 6 solved using the different versions of the ARoe solver (left) and of the HLLS solver (right). Methods ARoe1 and HLLS1 are plotted in blue, ARo2 and HLLS2 in red and ARoe3 and HLLS3 in yellow. (For interpretation of the references to color in this figure legend, the reader is referred to the web version of this article.)

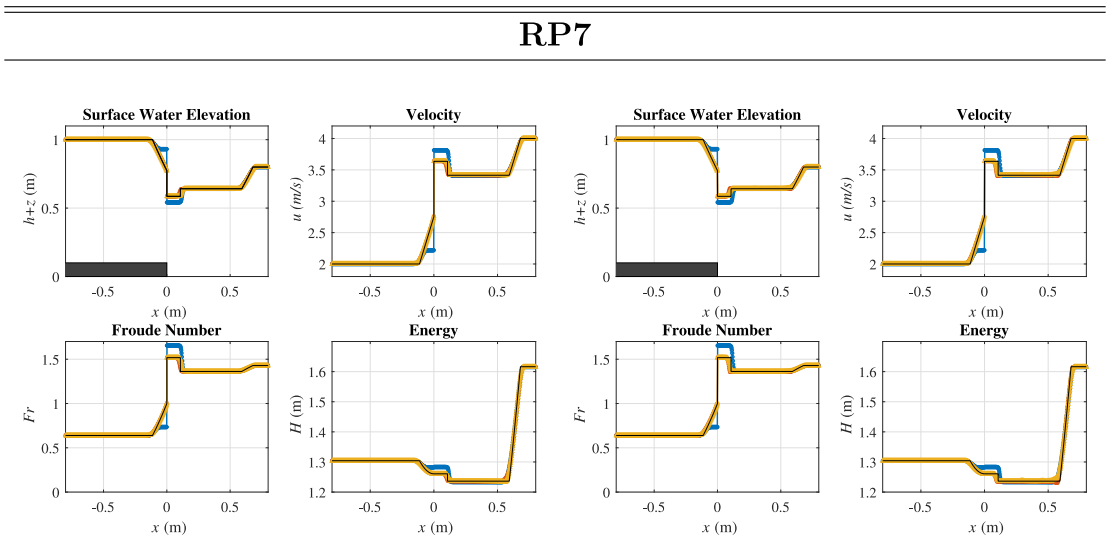

Fig. 13. RP 7 solved using the different versions of the ARoe solver (left) and of the HLLS solver (right). Methods ARoe1 and HLLS1 are plotted in blue, ARo2 and HLLS2 in red and ARoe3 and HLLS3 in yellow. (For interpretation of the references to color in this figure legend, the reader is referred to the web version of this article.)

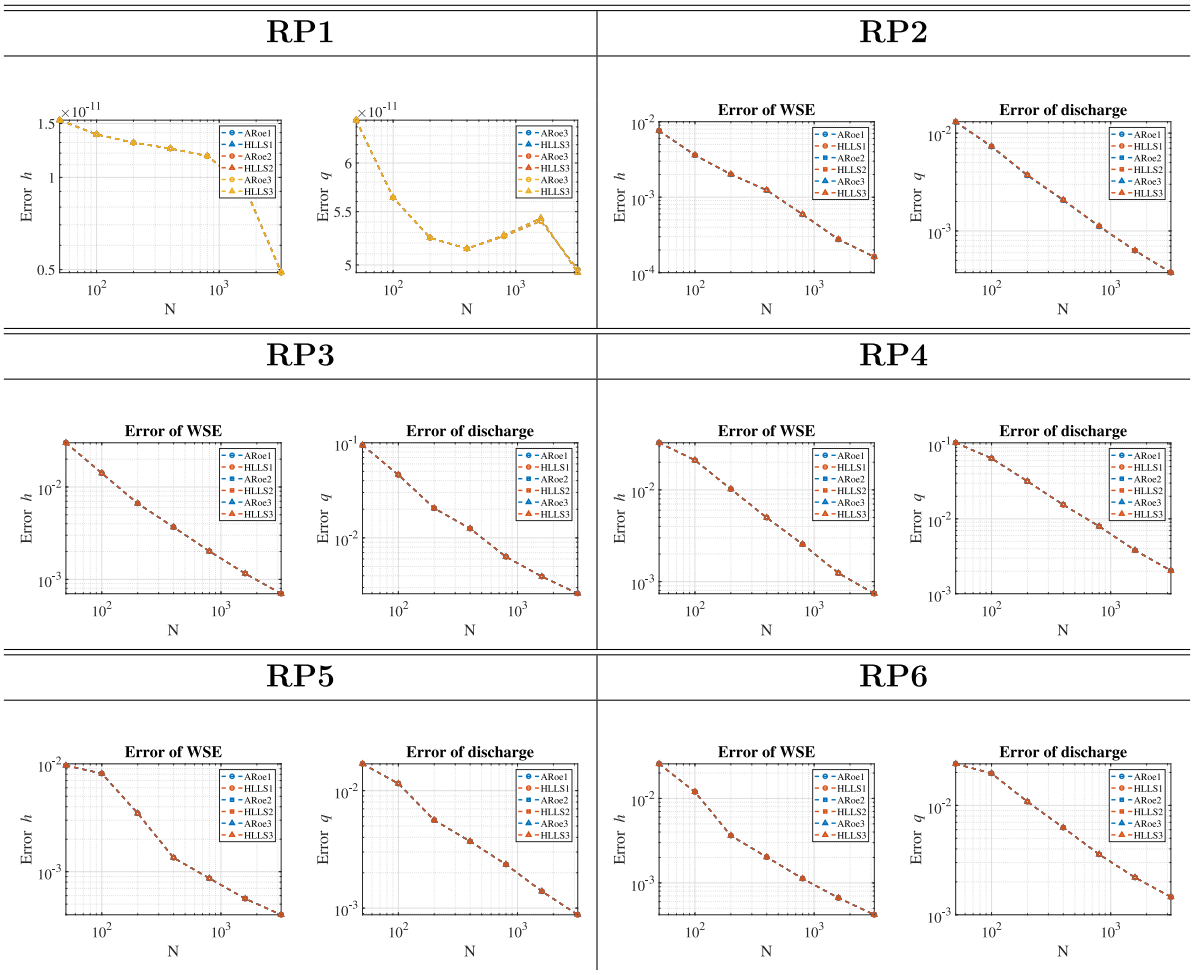

Fig. 14. Errors of RPs 1 trough 6 solved using the different versions of the ARoe solver (left) and of the HLLS solver (right).

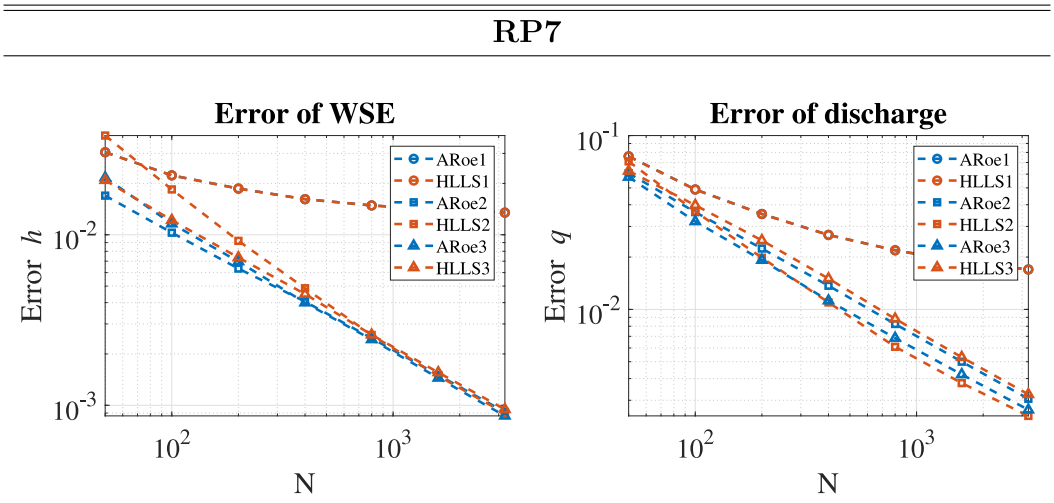

Fig. 15. RP 7 solved using the different versions of the ARoe solver (left) and of the HLLS solver (right).

Table 3
Boundary conditions in each bump case.

		h (m)		q (m^2/s)	
		$x = 0$	$x = L$	$x = 0$	$x = L$
C1	Subcritical	Free	2.0	4.42	Free
C2	Transcritical	Free	Free	1.53	Free
C3	Transcritical with shock	Free	0.33	0.18	Free

It is almost impossible that the jump falls exactly on the wall between cells. This problem is unrelated to any of the issues discussed in this paper and therefore all these methods behave identically.

RP 7 is specially relevant because it contains a transcritical rarefaction at the bed step. The initial discontinuity causes the left side of the RP to be continuously accelerated towards the right, increasing its Froude number until it reaches the critical point Fr = 1 at the bed discontinuity. The HLLS solver in [17] was unable to match this solution, while the ARoe solver with an Entropy fix could. Fig. 13 shows that the analytical solution is matched by the ARoe solver as long as the entropy is fixed: both the simplified fix and the full fix, pictured at the left in red and yellow respectively, yield the correct solution. The HLLS solver shows that the key to obtain the right solution is to allow the choice of waves between the eigenvalues evaluated at the adjacent cells and those obtained by using the Roe-averages, as done in HLLS2 and HLLS3. It seems that the choice of linearized Jacobian does not have an effect on the solution in a dynamic case such as this one.

6.2. Flow over a bump

The test case of a steady flow over a bump has been selected to tests these methods because, if the correct boundary conditions are given, a critical point of Fr = 1 develops at the cusp of the bump. It has been widely used [53–55,17] since its exact solution is readily available. A domain of length $L = 25$ m is set up with a bed elevation defined as:

$$z(x) = \begin{cases} 0.2 - 0.05(x-10)^2 & \text{if} \quad 8 \leqslant x \leqslant 12 \\ 0 & \text{otherwise} \end{cases}, \tag{123}$$

with different boundary conditions which define different steady solutions, as shown in Table 3.

To work well, the solvers must preserve the steady solution and, importantly, if a regime transition is present, they should replicate Fr = 1 to machine precision at the point of maximum bed elevation.

Case C1 considers subcritical flow in the entire domain, determined by a fixed discharge upstream and a fixed water depth downstream. Fig. 16 (top-left) shows that all versions of the ARoe solver manage to maintain the steady state in agreement with the analytical solution. This is to be expected in the ARoe, since no regime transition is present. Therefore, the entropy fix, which is what differentiates the versions, does not come into play.

On the other hand, the top-right plot of Fig. 16 shows that the third version of the HLLS solver does not maintain the steady state correctly. The deviation appears at $x = 8$ m, exactly where the effect of the source starts. Since the effect of the source term in the HLLS solver is applied through the $\bar{\mathbf{H}}$ term, it seems that approximating the determinant of the Jacobian by $\sigma_L \sigma_R$ unbalances the contribution of the source term to the fluxes, provoking $\mathbf{F}^+_{i+\frac{1}{2}} - \mathbf{F}^-_{i+\frac{1}{2}} - \bar{\mathbf{S}}_{i+\frac{1}{2}} \neq 0$, which produces inaccurate results. When the

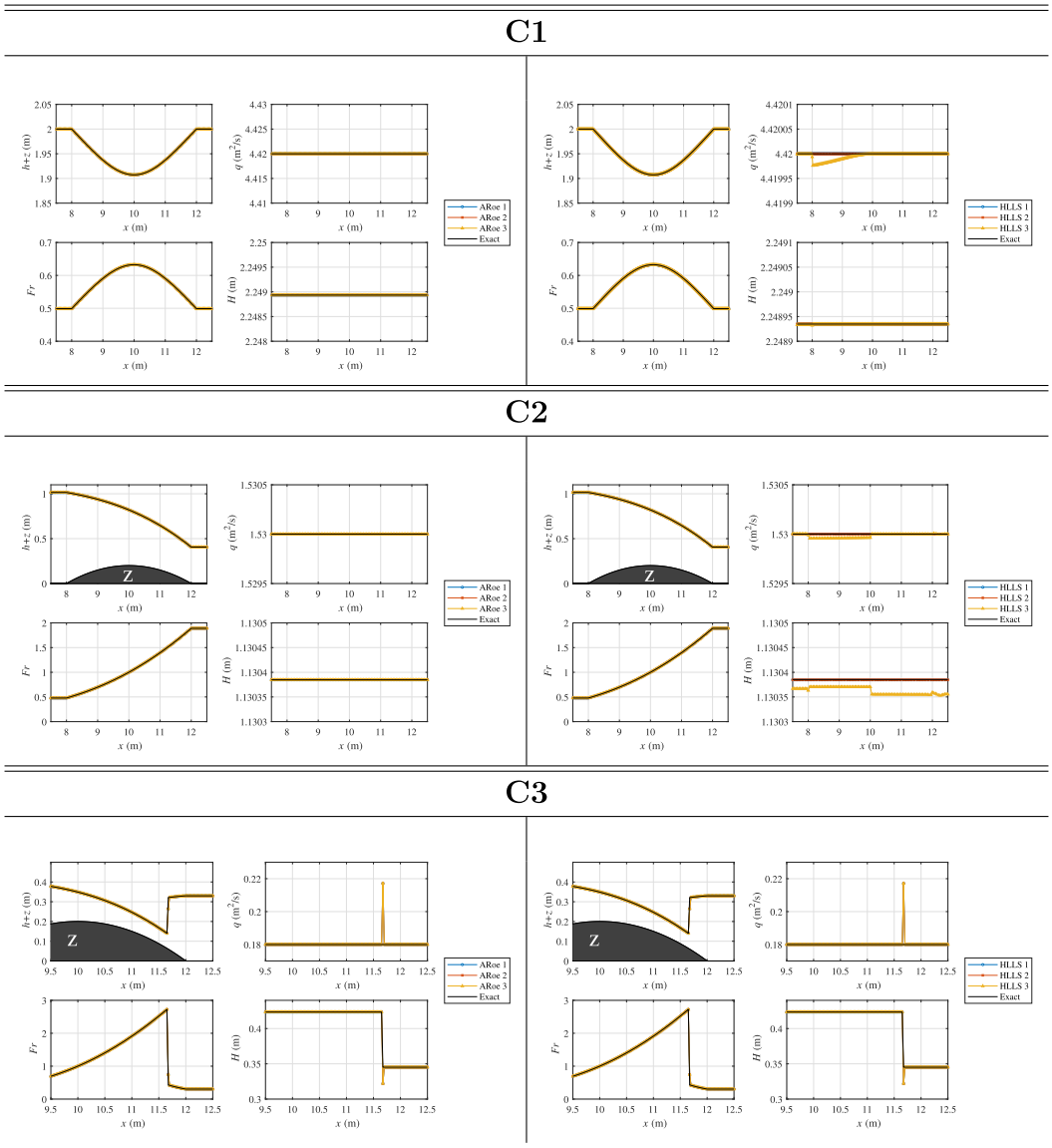

Fig. 16. All three instances (C1-C3) of the bump configuration solved using the different versions of the ARoe solver (left) and of the HLLS solver (right). Methods ARoe1 and HLLS1 are plotted in blue, ARo2 and HLLS2 in red and ARoe3 and HLLS3 in yellow. (For interpretation of the references to color in this figure legend, the reader is referred to the web version of this article.)

determinant of the Jacobian is approximated by $\tilde{\lambda}_1\tilde{\lambda}_2$ instead, the effect of the source term produces the correct results of constant discharge.

Table 4 shows the error computed as the L1 norm of the difference between the numerical solutions and the exact solution.

Case C2 includes a critical point where the flow regime changes from subcritical to supercritical. It is known [56] that the regime transition occurs at the cusp of the bump. Numerically, this means that the cell with maximum bed elevation will have $u_i = \sqrt{gh_i}$ such that $\mathrm{Fr}_i = 1$, but only if the mesh includes the cell with maximum z. Otherwise, convergence to the analytical solution is impossible. As a consequence, the corrections presented in Sections 4 and 5 are here tested.

Fig. 16 (middle) shows that, again, all versions of the ARoe solver maintain the steady state in agreement with the analytical solution, even the data series ARoe 1, where no entropy fix is included. Again, only method HLLS 3 fails to reproduce the exact solution whenever the bed elevation contributes to the source term. This keeps confirming that $\det \bar{\mathbf{J}} = \sigma_L\sigma_R$ is a bad approximation and even more so in a case where a certain cell is known to fulfill $u_i = \sqrt{gh_i}$ since $\sigma_L = 0$ and the approximate Jacobian cannot be inverted to obtain the $\bar{\mathbf{H}}$ term. This is also reflected in Table 4.

In case C3, a constant water depth is used as downstream boundary condition forcing the flow to be in the subcritical regime, while a constant discharge is imposed upstream. The acceleration after the bump causes a critical transition at the cusp, but the

Table 4
Error between the exact and the different numerical solution, computed using the L1 norm for all 3 instances of the bump configuration.

	C1		C2		C3	
	h (m)	q (m^2/s)	h (m)	q (m^2/s)	h (m)	q (m^2/s)
ARoe1	0.0	0.0	0.0	0.0	5.63e−05	3.76e−05
ARoe2	0.0	0.0	0.0	0.0	5.63e−05	3.76e−05
ARoe3	0.0	0.0	0.0	0.0	5.63e−05	3.76e−05
HLLS1	0.0	0.0	0.0	0.0	5.63e−05	3.76e−05
HLLS2	0.0	0.0	0.0	0.0	5.63e−05	3.76e−05
HLLS3	7.25e−07	1.05e−06	2.17e−05	7.37e−06	6.77e−05	4.52e−05

flow at the exit must be subcritical. This leads to a hydraulic jump that dissipates energy. As the energy is known both upstream and downstream of the jump, how much energy is dissipated can be known and an analytical solution is readily available to judge the results of the solvers.

In this case, Fig. 16 (bottom) shows how convergence to the exact solution is achieved by all methods except at the cell of the dissipative shock. This numerical defect appeared in RP6, in the previous section: failure to locate the hydraulic jump in the discrete mesh is causing the integral in the cell containing the shock to be wrong [52]. Table 4 shows that none of the methods actually achieve machine precision because of that. Except for the HLLS 3 data series, all solutions exhibit the same numerical error, on account of the defect generated by the hydraulic jump. The error of the HLLS 3 series is different due to its defects, but in any case, it is of the same order of magnitude because the error provoked by the jump still dominates.

7. Conclusions

The goal of this paper was two-fold. First, it aimed at clearly deriving the entropy fix of Harten–Hyman for the ARoe solver as formulated in [16], including source terms contributions. A complete formulation of the entropy fix has been given rigorously developing the $\lambda^{\leftarrow}$, $\lambda^{\rightarrow}$ terms in the presence of source terms for the first time, showing that a $\bar{\mathbf{H}}$ term can be introduced to establish a relation between the intermediate states across the local Riemann problem. This has been related to the classical Harten–Hyman fix in problems with source terms, and it has been shown that one reduces to the other in the steady limit. In addition to giving a better understanding of its formulation and of the place that the source terms have in it, the numerical experiments undertaken and exposed in Section 6 show that both implementations of the fix yield good results.

Second, a closer look to the HLLS method has been taken, exploring the different choices of waves and of the linearized Jacobian present in the source term contribution. It has been shown that, restricting σ_L, σ_R to only the Roe eigenvectors $\tilde{\lambda}_1$, $\tilde{\lambda}_2$ in cases with source term, as it was previously proposed in [25], is not necessary and it was in fact causing the HLLS solver to be less accurate than its ARoe counterpart in dynamic cases with transcritical rarefactions and bed elevation discontinuities. It was argued in [17] that a more sophisticated choice of waves would be necessary to produce accurate results capable of handling critical transitions like those of RP7 or the transcritical flow over a bump. Nevertheless, this paper shows the opposite. A simpler choice of waves achieves convergence to the analytical solution in the former. Additionally, it is suggested that a different determinant of the linearized Jacobian could be chosen to calculate the difference in the approximate solution across the inter-cell wall, labeled **H**. Previously [25] the Roe-averaged eigenvalues were used, which made sense since these were always chosen when source terms where present and the determinant of the Jacobian appears only in such cases. Nevertheless, by opening the choice of waves even when source terms are present, it seemed natural to allow this freedom to the determinant as well. However, the numerical results of the flow over a bump show that this provides the wrong solutions and unbalances the solver. A possible explanation for this defect is the fact that the choice of $\sigma_L\sigma_R$ is less precise at approximating the characteristic polynomial of the Jacobian evaluated at the inter-cell wall. This imprecision unbalances the contribution of the source term in the calculation of the flux, yielding slightly incorrect results that propagate as the calculation advances in time.

To conclude, the version of the entropy fix labeled **ARoe 2** is recommended henceforth due to its precision and comparative simplicity. The fact that fewer calculations need to be done to identify a transcritical rarefaction and perform the wave splitting while keeping the same precision as the more complex entropy fix is clearly an advantage. Regarding the HLLS solver, the choice of waves and of characteristic polynomial labeled **HLLS 2** is recommended henceforth. It is the only choice that solves correctly both the dynamic case of the transcritical RP and the flow over a bump in all regime combinations. With it, this work confirms that the HLLS solver can perform as well as the ARoe solver.

Declaration of competing interest

The authors declare that they have no known competing financial interests or personal relationships that could have appeared to influence the work reported in this paper.

Data availability

Data will be made available on request.

Acknowledgments

This work was funded by the Spanish Ministry of Universities under the grant FPU21/02876 and under the research project PGC2018-094341-B-I00. This work has also been partially funded by Gobierno de Aragón, Spain through Fondo Social Europeo (T32-20R and E24-17R, Feder 2019–2021).

Appendix A. Source term linearization

One of the key questions when solving this system of equation is how to formulate and integrate the source term. In this case, it accounts for the change in momentum caused by the varying geometry of the bed. Given a discretization so that every cell x_i has an associated constant bed elevation z_i, the channel can be thought of as a succession of steps. At each cell wall, there is a discontinuity of the bed and therefore a step that exerts a certain thrust. The source term is assumed to be constant in the timestep $[t^n, t^{n+1}]$ and acting only at cell walls. It is now a matter of finding a right formulation for it.

A.1. Differential linearization

The simplest possible formulation stems from assuming a hydrostatic pressure distribution which gives the differential formulation of the thrust

$$S^a = -\left(gh\frac{\partial z_b}{\partial x}\right)$$

which, if discretized

$$\bar{S}^a_{i+\frac{1}{2}} = -\left(g\bar{h}\Delta z\right)_{i+\frac{1}{2}} \tag{A.1}$$

where $\bar{h}_{i+\frac{1}{2}}$ is the average water height of the adjacent cells and $\Delta z_{\frac{1}{2}}$ is the size of the bed step, which can be positive for an increasing bed level or negative for a decreasing bed level. This, in combination with the negative sign in the expression, yields a positive thrust if water moves towards a lower bed section and a negative thrust if it moves towards a higher bed section, which agrees with common sense.

A.2. Integral linearization

The differential formulation, while useful, does not consider the whole picture. Indeed, it might be the case that at a certain cell wall, the total water height $z_i + h_i$ is lower that the height of the bed at the next cell $z_{i+1} > i$. In such a case, only the height of the step covered by fluid would need to be into account when evaluating the thrust. Including this possibility into the linearization of the source term requires changing the expression of $\bar{S}$

$$\bar{S}^b_{i+\frac{1}{2}} = -g\left(h_j - \frac{|\delta\zeta|}{2}\right)_{i+\frac{1}{2}} \delta\zeta_{i+\frac{1}{2}} \tag{A.2}$$

where the index j gives which cell around the discontinuity has a lower bed level

$$j = \begin{cases} i & \text{if } z_i \leqslant z_{i+1} \\ i+1 & \text{if } z_i > z_{i+1} \end{cases}$$

and where $\delta\zeta$ controls whether the whole step is under water or not

$$\delta\zeta = \begin{cases} h_i & \text{if } z_i \leqslant z_{i+1} \text{ and } (z_i + h_i) < z_{i+1} \\ -h_{i+1} & \text{if } z_i > z_{i+1} \text{ and } (z_{i+1} + h_{i+1}) < z_i \\ \delta z & \text{otherwise} \end{cases}$$

This is a more complete formulation which allows for some better results in cases with larger discontinuities in the bed step [16].

A.3. Linearization based on energy conservation

The integral and differential formulations seem to work well in general even if they do not take into account some physical effects present when a flow encounters a positive or negative step. Phenomena including non-hydrostatic pressure caused by the vertical acceleration of the fluid that climbs upwards or downwards is not present in a simplified model such as this one. However, there are other ways to ensure that the source term contribution is as accurate as possible [17]. Starting from a stationary state in a one-dimensional Shallow Water system, the conservation of momentum yields

$$\frac{\partial}{\partial x}\left(hu^2 + \frac{1}{2}gh^2\right) = S, \tag{A.3}$$

where S is the non-linearized version of the source term. Integration leads to

$$\delta\left(hu^2 + \frac{1}{2}gh^2\right)_{i+\frac{1}{2}} = \bar{S}_{i+\frac{1}{2}}, \tag{A.4}$$

where the left-hand side is the difference between the total momenta in cells $i+1$ and i, and the right-hand side is the linearized source term. As explained, there are different ways to formulate the linearization, based on arguments of hydrostatics. However, a possible approach is to formulate a linear combination of both methods using a weight parameter $\mathcal{A}$, so that a better approximation could be

$$\bar{S}^e_{i+\frac{1}{2}} = (1-\mathcal{A})\bar{S}^a_{i+\frac{1}{2}} + \mathcal{A}\bar{S}^b_{i+\frac{1}{2}}. \tag{A.5}$$

In order to find the weight parameter $\mathcal{A}$, energy conservation is enforced across the discontinuity in the channel bed, which is equivalent to assuming that there is neither friction nor dissipation at any hydraulic jumps. Thus, mechanical energy

$$H_i = \frac{u_i^2}{2g} + h_i + z_i \tag{A.6}$$

must be equal in both cells around the discontinuity. This can be written simply using a discretization

$$\frac{1}{2g}\delta(u^2)_{i+\frac{1}{2}} + \delta h_{i+\frac{1}{2}} + \delta z_{i+\frac{1}{2}} = 0. \tag{A.7}$$

On the other hand, the discretized equation of momentum between cells i and $i+1$ has already been formulated in (A.4) and its source term can be approximated by the linearization shown in Eq. (A.5)

$$\delta(hu^2)_{i+\frac{1}{2}} + \frac{1}{2}g\delta(h^2)_{i+\frac{1}{2}} = \bar{S}_{i+\frac{1}{2}} = (1-\mathcal{A})\bar{S}^a_{i+\frac{1}{2}} + \mathcal{A}\bar{S}^b_{i+\frac{1}{2}}. \tag{A.8}$$

Rearranging and using $\frac{1}{2}\delta(h^2) = \bar{h}\delta h$, where $\bar{h}$ is the arithmetic average of depths h_i and h_{i+1}, and the definition of the differential source term $\bar{S}^a_{i+\frac{1}{2}}$

$$\mathcal{A} = \frac{\delta(hu^2)_{i+\frac{1}{2}} + g\bar{h}\delta(h+z)_{i+\frac{1}{2}}}{\left(\bar{S}^b - \bar{S}^a\right)_{i+\frac{1}{2}}}. \tag{A.9}$$

It must be noted that while the $\mathcal{A}$ parameter can be isolated in this expression using just the discrete momentum equation, it would not be uniquely determined due to the fact that it is an approximation from the differential momentum equation that requires the integration of the source term. Thus, to determine an appropriate parameter the energy Eq. (A.7) must be introduced. Since this equation can be integrated exactly without approximation, it ensures the correct parameter is found in exchange for a loss of generality. Indeed, energy is conserved in situations without friction or hydraulic jumps. The latter case, present when a regime transition occurs, needs to be solved with the integral or differential approximations of the source term.

Thus, using and the discrete energy Eq. (A.7), the weight parameter $\mathcal{A}_E$ can be written

$$\mathcal{A}_E = \frac{\delta(hu^2)_{i+\frac{1}{2}} + \frac{1}{2}\bar{h}\delta(u^2)_{i+\frac{1}{2}}}{\left(\bar{S}^b - \bar{S}^a\right)_{i+\frac{1}{2}}}. \tag{A.10}$$

This expression needs to be include an exception where hydraulic jumps occur, which can be formulated as a conditional

$$\mathcal{A} = \begin{cases} \mathcal{A}_E & \text{if } u_{i+1}u > 0 \text{ and } |\mathrm{Fr}_{i+1}| < 1 \text{ and } |\mathrm{Fr}_i| < 1 \\ \mathcal{A}_E & \text{if } u_{i+1}u > 0 \text{ and } |\mathrm{Fr}_{i+1}| > 1 \text{ and } |\mathrm{Fr}_i| > 1 \\ 1 & \text{otherwise,} \end{cases}$$

where the first two cases account for a flow that moves in the same direction and which has the same regime at both sides of the discontinuity. The third case accounts for regime changes and therefore The question that arises now is whether this parameter is bounded in a certain interval. Since $\bar{S}^e$ is formulated as a weighted average, it is logical to think that the weight parameter should be contained in the interval $[0,1]$ [17]. However, this is not necessarily the case. In fact, it has been witnessed in certain test cases that $\mathcal{A}_E$ can fall outside of this interval. If it was constrained to it, it would mean that the value of the linearized source term needs to be bounded by the values obtained using the integral and differential methods. However, there is no reason to think that a value outside of this range is unacceptable. While this is an interesting question, it falls outside of the scope of this paper.

Appendix B. Weak solutions in the supercritical regime

The piecewise solution given by (25) is not valid if the eigenvalues $\bar{\lambda}_1$, $\bar{\lambda}_2$ have the same sign, either positive or negative, where the regime is said to be supercritical. Then, the weak solution is given by:

$$\hat{\mathbf{U}}(x',\Delta t) = \begin{cases} \mathbf{U}_i & if \quad x' < \bar{\lambda}_1\Delta t \\ \mathbf{U}_i^- & if \quad \bar{\lambda}_1\Delta t < x' < \bar{\lambda}_2\Delta t \\ \mathbf{U}_i^+ & if \quad \bar{\lambda}_2\Delta t < x' < 0 \\ \mathbf{U}_{i+1} & if \quad x' > 0 \end{cases}, \tag{B.1}$$

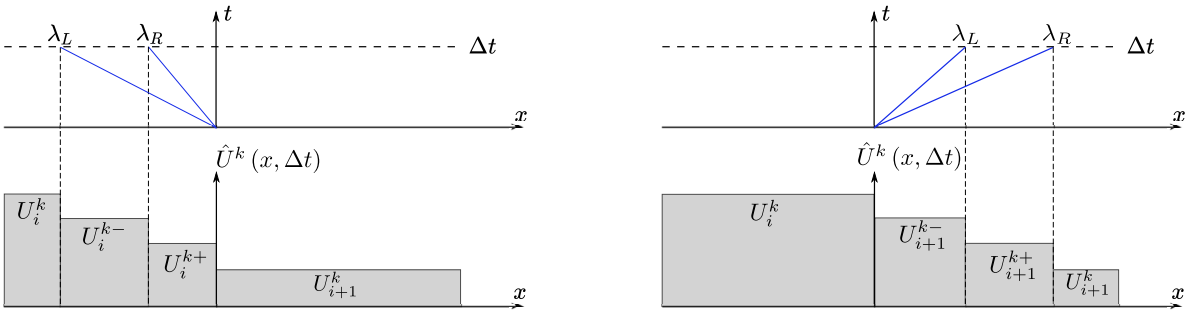

Fig. B.17. Piecewise solution $\hat{\mathbf{U}}(x,\Delta t)$ in the supercritical case.

if $\bar{\lambda}_1 < \bar{\lambda}_2 < 0$ and

$$\hat{\mathbf{U}}(x',\Delta t) = \begin{cases} \mathbf{U}_i & if \quad x' < 0 \\ \mathbf{U}_{i+1}^- & if \quad 0 < x' < \bar{\lambda}_1 \Delta t \\ \mathbf{U}_{i+1}^+ & if \quad \bar{\lambda}_1 \Delta t < x' < \bar{\lambda}_2 \Delta t \\ \mathbf{U}_{i+1} & if \quad x' > \bar{\lambda}_2 \Delta t \end{cases}, \tag{B.2}$$

if $0 < \bar{\lambda}_1 < \bar{\lambda}_2$ with intermediate states defined as:

$$\mathbf{U}_i^- = -\frac{1}{(\bar{\lambda}_1 - \bar{\lambda}_2)\Delta t} \int_{\bar{\lambda}_1 \Delta t}^{\bar{\lambda}_2 \Delta t} \mathbf{U}(x',\Delta t) dx, \qquad \mathbf{U}_i^+ = -\frac{1}{\bar{\lambda}_2 \Delta t} \int_{\bar{\lambda}_2 \Delta t}^{0} \mathbf{U}(x',\Delta t) dx, \tag{B.3}$$

if $\bar{\lambda}_1 < \bar{\lambda}_2 < 0$ and:

$$\mathbf{U}_{i+1}^- = \frac{1}{\bar{\lambda}_1 \Delta t} \int_{0}^{\bar{\lambda}_1 \Delta t} \mathbf{U}(x',\Delta t) dx, \qquad \mathbf{U}_{i+1}^+ = \frac{1}{(\bar{\lambda}_2 - \bar{\lambda}_1)\Delta t} \int_{\bar{\lambda}_1 \Delta t}^{\bar{\lambda}_2 \Delta t} \mathbf{U}(x',\Delta t) dx, \tag{B.4}$$

for $0 < \bar{\lambda}_1 < \bar{\lambda}_2$. The subscript indicates on which side of the inter-cell wall these states lie.

B.1. The supercritical case in the HLLS method

If the regime is supercritical both intermediate states are located on the same side of the inter-cell wall as shown in Fig. B.17. In this case, the approximate central states of the weak solution are given by:

$$\mathbf{F}_{i+\frac{1}{2}}^+ = \mathbf{F}_{i+1}, \qquad \mathbf{F}_{i+\frac{1}{2}}^- = \mathbf{F}_{i+1} - \bar{\mathbf{S}}_{i+\frac{1}{2}}, \tag{B.5}$$

if $\sigma_R < 0$ and $\sigma_L < 0$, and

$$\mathbf{F}_{i+\frac{1}{2}}^+ = \mathbf{F}_{i+1} + \bar{\mathbf{S}}_{i+\frac{1}{2}}, \qquad \mathbf{F}_{i+\frac{1}{2}}^- = \mathbf{F}_i, \tag{B.6}$$

if $\sigma_R > 0$ and $\sigma_L > 0$.

Appendix C. Inhomogeneous right transcritical rarefaction

Fig. 8 (right) shows a right transcritical rarefaction with the bed source term acting at $x' = 0$. This time, it is assumed that the rarefaction is bounded between λ_2^- and λ_2^{i+1}, where:

$$\lambda_2^- = \lambda_2(\mathbf{U}_i^-) = u_i^- + \sqrt{g h_i^-} \qquad \text{and} \qquad \lambda_2^{i+1} = \lambda_2(\mathbf{U}_{i+1}) = u_{i+1} + \sqrt{g h_{i+1}}, \tag{C.1}$$

and fulfills:

$$\lambda_2^- < 0 < \lambda_2^{i+1}. \tag{C.2}$$

Again, the rarefaction can be better represented by two new constant states separated by the contact wave, whose expressions are given by the following average solutions:

$$\mathbf{U}_{TrC}^- = \frac{1}{\Delta x} \int_{\lambda_2^- \Delta t}^{0} \mathbf{U}(x,\Delta t) dx, \quad \mathbf{U}_{TrC}^+ = \frac{1}{\Delta x} \int_{0}^{\lambda_2^{i+1} \Delta t} \mathbf{U}(x,\Delta t) dx. \tag{C.3}$$

If $\tilde{\lambda}_2$ fulfills condition (C.2), the rarefaction is to the right and $\tilde{\lambda}_2$ needs to be split in order to generate a weak solution with a structure as shown in Fig. 10 (right). By integrating (22) in the control volume $[\lambda_2^- \Delta t, \lambda_2^{i+1} \Delta t]$, a consistency equation relating $\mathbf{U}_{TrC}^-$ and $\mathbf{U}_{TrC}^+$ can be found:

$$-(\tilde{\lambda}_1 - \lambda_2^-)\mathbf{U}_i^- - \lambda_2^- \mathbf{U}_{TrC}^+ + \lambda_2^{i+1}\mathbf{U}_{TrC}^+ + \tilde{\lambda}_2 \mathbf{U}_i - \lambda_2^{i+1}\mathbf{U}_{i+1} + (\mathbf{F}_{i+1} - \mathbf{F}_i - \tilde{\mathbf{S}}_{i+\frac{1}{2}}) = 0, \tag{C.4}$$

From this equation, the same process is repeated and the $\tilde{\mathbf{H}}$ term is introduced in the same way to finally obtain fluxes:

$$\mathbf{F}_{TrC}^+ = \mathbf{F}_{i+1} - \lambda_2^- \frac{\lambda_2^{i+1} - \tilde{\lambda}_2}{\lambda_2^{i+1} - \lambda_2^-}\left(\tilde{\alpha}_2 - \frac{\beta_2}{\tilde{\lambda}_2}\right)\tilde{\mathbf{e}}^2 - \frac{\lambda_2^{i+1}\lambda_2^-}{\lambda_2^{i+1} - \lambda_2^-}\tilde{\mathbf{H}} \tag{C.5}$$

$$\mathbf{F}_{TrC}^- = \mathbf{F}_{\mathbf{L}}^- - \lambda_2^{i+1} \frac{\tilde{\lambda}_2 - \lambda_2^-}{\lambda_2^{i+1} - \lambda_2^-}\left(\tilde{\alpha}_2 - \frac{\beta_2}{\tilde{\lambda}_2}\right)\tilde{\mathbf{e}}^2 - \frac{\lambda_2^-\lambda_2^{i+1}}{\lambda_2^{i+1} - \lambda_2^-}\tilde{\mathbf{H}}. \tag{C.6}$$

from which the new split waves can be naturally defined as:

$$\lambda_2^{\rightarrow} = \lambda_2^{i+1}\frac{\tilde{\lambda}_2 - \lambda_2^-}{\lambda_2^{i+1} - \lambda_2^-} \qquad \beta_2^{\rightarrow} = \frac{\lambda_2^{i+1}}{\tilde{\lambda}_2}\frac{\tilde{\lambda}_2 - \lambda_2^-}{\lambda_2^{i+1} - \lambda_2^-}\beta_2 = \frac{\lambda_2^{\rightarrow}}{\tilde{\lambda}_2}\beta_2 \tag{C.7}$$

$$\lambda_2^{\leftarrow} = \lambda_2^-\frac{\lambda_2^{i+1} - \tilde{\lambda}_2}{\lambda_2^{i+1} - \lambda_2^-} \qquad \beta_2^{\leftarrow} = \frac{\lambda_2^-}{\tilde{\lambda}_2}\frac{\lambda_2^{i+1} - \tilde{\lambda}_2}{\lambda_2^{i+1} - \lambda_2^-}\beta_2 = \frac{\lambda_2^{\leftarrow}}{\tilde{\lambda}_2}\beta_2. \tag{C.8}$$

So the fluxes are computed as:

$$\mathbf{F}_{i+\frac{1}{2}}^+ = \mathbf{F}_{TrC}^+ = \mathbf{F}_{i+1} - \left(\lambda_2^{\leftarrow}\tilde{\alpha}_2 - \beta_2^{\leftarrow}\right)\tilde{\mathbf{e}}^2 - \frac{\lambda_2^{i+1}\lambda_2^-}{\lambda_2^{i+1} - \lambda_2^-}\tilde{\mathbf{H}}_{i+\frac{1}{2}} \tag{C.9}$$

$$\mathbf{F}_{i+\frac{1}{2}}^- = \mathbf{F}_{TrC}^- = \mathbf{F}_i + \left(\tilde{\lambda}_1\tilde{\alpha}_1 - \beta_1\right)\tilde{\mathbf{e}}^1 - \left(\lambda_2^{\rightarrow}\tilde{\alpha}_2 - \beta_2^{\rightarrow}\right)\tilde{\mathbf{e}}^2 - \frac{\lambda_2^-\lambda_2^{i+1}}{\lambda_2^{i+1} - \lambda_2^-}\tilde{\mathbf{H}}_{i+\frac{1}{2}}. \tag{C.10}$$

References

[1] T.T. Dullo, S. Gangrade, M. Morales-Hernández, M.B. Sharif, A.J. Kalyanapu, S.-C. Kao, S. Ghafoor, M. Ashfaq, Assessing climate change-induced flood risk in the Conasauga river watershed: An application of ensemble hydrodynamic inundation modeling, Nat. Hazard. Earth Syst. Sci. Discuss. 2020 (2020) 1–54.

[2] W. Kron, Flood disasters–a global perspective, Water Policy 17 (S1) (2015) 6–24.

[3] W.J. Ripple, C. Wolf, J.W. Gregg, K. Levin, J. Rockström, T.M. Newsome, M.G. Betts, S. Huq, B.E. Law, L. Kemp, et al., World scientists' warning of a climate emergency 2022, 2022, Oxford University Press.

[4] P. Vallés, I. Echeverribar, J. Mairal, S. Martínez-Aranda, J. Fernández-Pato, P. García-Navarro, 2D numerical simulation of floods in the Ebro river and analysis of boundary conditions to model the Mequinenza reservoir dam, GeoHazards 4 (2023) 136156.

[5] P.G. LeFloch, M.D. Thanh, The Riemann problem for the shallow water equations with discontinuous topography, Commun. Math. Sci. 5 (4) (2007) 865–885.

[6] P. Glaister, Approximate Riemann solutions of the shallow water equations, J. Hydraul. Res. 26 (3) (1988) 293–306.

[7] A. Bermudez, M.E. Vazquez, Upwind methods for hyperbolic conservation laws with source terms, Comput. & Fluids 23 (8) (1994) 1049–1071.

[8] J.M. Greenberg, A.-Y. LeRoux, A well-balanced scheme for the numerical processing of source terms in hyperbolic equations, SIAM J. Numer. Anal. 33 (1) (1996) 1–16.

[9] P. Garcia-Navarro, M.E. Vazquez-Cendon, On numerical treatment of the source terms in the shallow water equations, Comput. & Fluids 29 (8) (2000) 951–979.

[10] A. Harten, J.M. Hyman, Self adjusting grid methods for one-dimensional hyperbolic conservation laws, J. Comput. Phys. 50 (2) (1983) 235–269.

[11] R.J. LeVeque, et al., Finite Volume Methods for Hyperbolic Problems, vol. 31, Cambridge University Press, 2002.

[12] Y. Xing, C.-W. Shu, S. Noelle, On the advantage of well-balanced schemes for moving-water equilibria of the shallow water equations, J. Sci. Comput. 48 (1–3) (2011) 339–349.

[13] Y. Cheng, A. Kurganov, Moving-water equilibria preserving central-upwind schemes for the shallow water equations, Commun. Math. Sci. 14 (6) (2016) 1643–1663.

[14] V. Caleffi, A. Valiani, Well balancing of the SWE schemes for moving-water steady flows, J. Comput. Phys. 342 (2017) 85–116.

[15] S. Noelle, Y. Xing, C.-W. Shu, High-order well-balanced finite volume WENO schemes for shallow water equation with moving water, J. Comput. Phys. 226 (1) (2007) 29–58.

[16] J. Murillo, P. García-Navarro, Weak solutions for partial differential equations with source terms: Application to the shallow water equations, J. Comput. Phys. 229 (11) (2010) 4327–4368.

[17] J. Murillo, P. García-Navarro, Energy balance numerical schemes for shallow water equations with discontinuous topography, J. Comput. Phys. 236 (2013) 119–142.

[18] D.L. George, Augmented Riemann solvers for the shallow water equations over variable topography with steady states and inundation, J. Comput. Phys. 227 (6) (2008) 3089–3113.

[19] P.L. Roe, Approximate Riemann solvers, parameter vectors, and difference schemes, J. Comput. Phys. 43 (2) (1981) 357–372.

[20] A. Harten, P.D. Lax, B.v. Leer, On upstream differencing and Godunov-type schemes for hyperbolic conservation laws, SIAM Rev. 25 (1) (1983) 35–61.

[21] E.F. Toro, A. Chakraborty, The development of a Riemann solver for the steady supersonic Euler equations, Aeronaut. J. 98 (979) (1994) 325–339.

[22] E.F. Toro, M. Spruce, W. Speares, Restoration of the contact surface in the HLL-Riemann solver, Shock Waves 4 (1994) 25–34.

[23] E.F. Toro, The hllc riemann solver, Shock Waves 29 (8) (2019) 1065–1082.

[24] E.F. Toro, L.O. Müller, A. Siviglia, Bounds for wave speeds in the Riemann problem: Direct theoretical estimates, Comput. & Fluids 209 (2020) 104640.

[25] J. Murillo, P. García-Navarro, Augmented versions of the HLL and HLLC Riemann solvers including source terms in one and two dimensions for shallow flow applications, J. Comput. Phys. 231 (20) (2012) 6861–6906.

[26] A. Lacasta, M. Morales-Hernández, J. Murillo, P. García-Navarro, GPU implementation of the 2D shallow water equations for the simulation of rainfall/runoff events, Environ. Earth Sci. 74 (2015) 7295–7305.
[27] M. Morales-Hernández, J. Murillo, P. García-Navarro, The formulation of internal boundary conditions in unsteady 2-D shallow water flows: Application to flood regulation, Water Resour. Res. 49 (1) (2013) 471–487.
[28] J. Murillo, B. Latorre, P. García-Navarro, A Riemann solver for unsteady computation of 2D shallow flows with variable density, J. Comput. Phys. 231 (14) (2012) 4775–4807.
[29] C. Juez, J. Murillo, P. García-Navarro, One-dimensional Riemann solver involving variable horizontal density to compute unsteady sediment transport, J. Hydraul. Eng. 142 (3) (2016) 04015056.
[30] J. Murillo, S. Martinez-Aranda, A. Navas-Montilla, P. García-Navarro, Adaptation of flux-based solvers to 2D two-layer shallow flows with variable density including numerical treatment of the loss of hyperbolicity and drying/wetting fronts, J. Hydroinform. 22 (5) (2020) 972–1014.
[31] S. Martínez-Aranda, J. Murillo, M. Morales-Hernández, P. García-Navarro, Novel discretization strategies for the 2D non-Newtonian resistance term in geophysical shallow flows, Eng. Geol. 302 (2022) 106625.
[32] J. Murillo, P. García-Navarro, Wave Riemann description of friction terms in unsteady shallow flows: Application to water and mud/debris floods, J. Comput. Phys. 231 (4) (2012) 1963–2001.
[33] C. Juez, D. Caviedes-Voullième, J. Murillo, P. García-Navarro, 2D dry granular free-surface transient flow over complex topography with obstacles. Part II: Numerical predictions of fluid structures and benchmarking, Comput. Geosci. 73 (2014) 142–163.
[34] S. Martínez-Aranda, J. Murillo, P. García-Navarro, A GPU-accelerated efficient simulation tool (EST) for 2D variable-density mud/debris flows over non-uniform erodible beds, Eng. Geol. 296 (2022) 106462.
[35] C. Juez, S. Soares-Frazao, J. Murillo, P. García-Navarro, Experimental and numerical simulation of bed load transport over steep slopes, J. Hydraul. Res. 55 (4) (2017) 455–469.
[36] C. Juez, C. Ferrer-Boix, J. Murillo, M.A. Hassan, P. García-Navarro, A model based on hirano-exner equations for two-dimensional transient flows over heterogeneous erodible beds, Adv. Water Resour. 87 (2016) 1–18.
[37] I. Echeverribar, S. Martínez-Aranda, J. Fernández-Pato, P. García-Navarro, A GPU-based 2D viscous flow model with variable density and heat exchange, Adv. Eng. Softw. 175 (2023) 103340.
[38] M. Morales-Hernández, M.B. Sharif, A. Kalyanapu, S.K. Ghafoor, T.T. Dullo, S. Gangrade, S.-C. Kao, M.R. Norman, K.J. Evans, TRITON: A multi-GPU open source 2D hydrodynamic flood model, Environ. Model. Softw. 141 (2021) 105034.
[39] A. Navas-Montilla, J. Murillo, 2D well-balanced augmented ADER schemes for the shallow water equations with bed elevation and extension to the rotating frame, J. Comput. Phys. 372 (2018) 316–348.
[40] A. Navas-Montilla, P. Solán-Fustero, J. Murillo, P. García-Navarro, Discontinuous Galerkin well-balanced schemes using augmented Riemann solvers with application to the shallow water equations, J. Hydroinform. 22 (5) (2020) 1038–1058.
[41] M.A. Alves, P.J. Oliveira, F.T. Pinho, Numerical methods for viscoelastic fluid flows, Annu. Rev. Fluid Mech. 53 (2021) 509–541.
[42] F. Bellamoli, L.O. Müller, E.F. Toro, A numerical method for junctions in networks of shallow-water channels, Appl. Math. Comput. 337 (2018) 190–213.
[43] J. Murillo, A. Navas-Montilla, P. García-Navarro, Formulation of exactly balanced solvers for blood flow in elastic vessels and their application to collapsed states, Comput. & Fluids 186 (2019) 74–98.
[44] J. Murillo, P. García-Navarro, A solution of the junction Riemann problem for 1D hyperbolic balance laws in networks including supersonic flow conditions on elastic collapsible tubes, Symmetry 13 (9) (2021) 1658.
[45] J. Burguete, P. García-Navarro, Efficient construction of high-resolution TVD conservative schemes for equations with source terms: Application to shallow water flows, Internat. J. Numer. Methods Fluids 37 (2) (2001) 209–248.
[46] P.G. LeFloch, M.D. Thanh, A Godunov-type method for the shallow water equations with discontinuous topography in the resonant regime, J. Comput. Phys. 230 (20) (2011) 7631–7660.
[47] E.F. Toro, Riemann Solvers and Numerical Methods for Fluid Dynamics: A Practical Introduction, Springer Science & Business Media, 2013.
[48] J. Murillo, A. Navas-Montilla, A comprehensive explanation and exercise of the source terms in hyperbolic systems using Roe type solutions. Application to the 1D-2D shallow water equations, Adv. Water Resour. 98 (2016) 70–96.
[49] S. Davis, Simplified second-order Godunov-type methods, SIAM J. Sci. Stat. Comput. 9 (3) (1988) 445–473.
[50] B. Einfeldt, On Godunov-type methods for gas dynamics, SIAM J. Numer. Anal. 25 (2) (1988) 294–318.
[51] B. Einfeldt, C.-D. Munz, P.L. Roe, B. Sjögreen, On Godunov-type methods near low densities, J. Comput. Phys. 92 (2) (1991) 273–295.
[52] A. Navas-Montilla, J. Murillo, Improved Riemann solvers for an accurate resolution of 1D and 2D shock profiles with application to hydraulic jumps, J. Comput. Phys. 378 (2019) 445–476.
[53] J.G. Zhou, D.M. Causon, C.G. Mingham, D.M. Ingram, The surface gradient method for the treatment of source terms in the shallow-water equations, J. Comput. Phys. 168 (1) (2001) 1–25.
[54] Q. Liang, A.G.L. Borthwick, Adaptive quadtree simulation of shallow flows with wet–dry fronts over complex topography, Comput. & Fluids 38 (2) (2009) 221–234.
[55] C. Berthon, F. Foucher, Efficient well-balanced hydrostatic upwind schemes for shallow-water equations, J. Comput. Phys. 231 (15) (2012) 4993–5015.
[56] F. Alcrudo, F. Benkhaldoun, Exact solutions to the Riemann problem of the shallow water equations with a bottom step, Comput. & Fluids 30 (6) (2001) 643–671.